

A statistical investigation of the mass discrepancy–acceleration relation

Harry Desmond[†]

*Kavli Institute for Particle Astrophysics and Cosmology and Physics Department, Stanford University, Stanford, CA 94305, USA;
SLAC National Accelerator Laboratory, Menlo Park, CA 94025, USA*

4 June 2022

ABSTRACT

We use the mass discrepancy–acceleration relation (the correlation between the ratio of dark-to-visible mass and acceleration in galaxies; MDAR) to test the galaxy–halo connection. We analyse the MDAR using a set of 14 statistics which quantify its four most important features: its shape, its scatter, the presence of a “characteristic acceleration scale,” and the correlation of its residuals with other galaxy properties. We construct an empirical framework for the galaxy–halo connection in Λ CDM to generate predictions for these statistics, starting with conventional correlations (halo abundance matching; AM) and introducing more where required. Comparing to the SPARC data (Lelli, McGaugh & Schombert 2016b), we find: 1) The approximate shape of the MDAR is readily reproduced by AM, and there is no evidence that the acceleration at which dark matter becomes negligible has less spread in the data than in AM mocks; 2) Even under conservative assumptions, AM significantly overpredicts the scatter in the relation and its normalisation at low acceleration, and furthermore positions dark matter too close to galaxies’ centres on average; 3) The MDAR affords 2σ evidence for a correlation of surface brightness with halo mass or concentration. Our analysis lays the groundwork for a bottom-up determination of the galaxy–halo connection from relations such as the MDAR, provides concrete statistical tests for specific galaxy formation models, and brings into sharper focus the relative evidence accorded by galaxy kinematics to Λ CDM and modified gravity alternatives.

Key words: galaxies: formation - galaxies: fundamental parameters - galaxies: haloes - galaxies: kinematics and dynamics - dark matter.

1 INTRODUCTION

The internal motions of galaxies are largely set by dark matter, which outweighs baryonic matter by at least five to one. A key goal of galaxy astrophysics is to relate the visible and dark mass in any given system, which to first order means determining the correlations between the structural parameters of galaxies (e.g. M_* , M_{gas} , R_{d} and Hubble type T) and those of dark matter haloes (e.g. M_{vir} , c , λ). This programme requires extensive observation of the rotation and velocity dispersion profiles of

galaxies and their baryonic mass distributions, combined with detailed dynamical modelling under a variety of assumptions about the galaxy–halo connection.

Traditional summaries of the relation between the baryonic mass distributions and internal motions of galaxies relate 1-point statistics of these functions, reducing the former to a total galaxy mass and size, and the latter to a single measure of velocity. These are the Tully–Fisher, mass–size and Faber–Jackson relations, along with the Fundamental Plane. More information, however, can be found in the full *radial* dependence of mass and velocity, and analysis of this dependence may be expected to afford not only a more stringent test of specific galaxy formation models, but also a richer foun-

[†] E-mail: harryd2@stanford.edu

dation for a bottom-up determination of the galaxy–halo connection.

The local correlation of dark and visible matter is usefully described by the ratio of enclosed dynamical mass (determined kinematically) to enclosed baryonic mass (determined photometrically). A proxy for this quantity is $V_{\text{tot}}^2(r)/V_{\text{bar}}^2(r)$, to which it is equal in the case of spherical mass distribution. $V_{\text{tot}}^2(r)/V_{\text{bar}}^2(r)$ is known as the “mass discrepancy” (McGaugh 1999), and will be denoted \mathcal{D} hereafter. In general, \mathcal{D} may be any function of position r within a galaxy, with parametric dependence on global galaxy properties X (e.g. M_* , M_{gas} , R_{d} , T). The full functional form of the mass discrepancy, $\mathcal{D}(r; X)$, is a kinematic parameterization of the relation between dark matter and baryons, and *a fortiori* of the galaxy–halo connection.

While in principle \mathcal{D} may have an arbitrary dependence on position, its utility is significantly enhanced by the fact that it is known to correlate strongly with acceleration $a(r)$ in all galaxies in which it has been measured in detail (Sanders 1990; McGaugh 1999, 2004; Tiret & Combes 2009; Famaey & McGaugh 2012; Janz et al. 2016). This allows us to focus our attention on $\mathcal{D}(a(r); X)$, which is known as the “mass discrepancy–acceleration relation” or MDAR. The tightness of this relation and its inclusion of information across a galaxy’s profile may be expected to make it among the most useful scaling relations for constraining models of the galaxy–halo connection. The value of the MDAR relative to 1-point summaries, regardless of tightness, may be approximately established by a simple counting argument: while the latter are limited to one data point per galaxy, the former contains as many data points as one can measure across the entirety of a galaxy’s rotation curve.

The aim of this paper is to construct a framework for using the MDAR to test galaxy formation models, and hence deduce the dynamically-relevant correlations of the galaxy–halo connection. Although the MDAR has been known observationally for decades, few studies have sought to systematically extract the information contained within it. The tightness of the relation is used by some to argue against all Λ CDM-based models of galaxy formation (McGaugh & de Blok 1998; McGaugh 1999, 2004; Kroupa 2012; McGaugh 2015; Wu & Kroupa 2015), where stochasticity in the galaxy–halo connection may be expected to introduce a significant scatter into the relation between \mathcal{D} and a . In addition, it is argued that the presence of a “characteristic acceleration” $a \approx 10^{-10} \text{ m s}^{-2}$ at which \mathcal{D} consistently becomes ~ 1 (indicating a dynamically-insignificant quantity of dark matter) is not compatible with standard galaxy formation. A generic galaxy–halo connection would predict a spread in \mathcal{D} at high a , and no clear transition in acceleration space between the dark matter and baryon-dominated regimes. Other authors, however, claim that the salient features of the MDAR arise naturally in Λ CDM models which have been tuned to match the Tully–Fisher (van den Bosch &

Dalcanton 2000) or $M_* - M_{\text{halo}}$, $M_* - R_{\text{d}}$ and $M_* - M_{\text{gas}}$ relations (Di Cintio & Lelli 2016), and consensus concerning the relation’s significance does not seem at hand. Furthermore, no study to date has systematically investigated the dependence of \mathcal{D} on global galaxy properties (X) at fixed a , or quantified the dependence of MDAR residuals on r .

Our specific task is twofold. First, we create a set of statistics to quantify four significant features of the MDAR: its shape, its scatter, the presence of a “characteristic acceleration,” and the correlation of its residuals with other variables (M_* , M_{gas} , R_{d} , T and r). This is motivated in part by the prevalence of purely qualitative claims in the literature concerning the compatibility of the MDAR with various models, from which it is difficult to determine the exact degree or nature of the agreement. Our statistics enable the conversion of verbal assertions into precise statistical comparisons, and we hope that they will sharpen future discussions of the MDAR regardless of theoretical perspective.

The salience of these statistical features, however, is best appreciated in the context of specific model expectations. Our second task, therefore, is to develop a semi-empirical framework in Λ CDM to generate predictions for the MDAR. We adopt a fully bottom-up methodology, beginning with the simplest and best motivated correlations between galaxy and halo variables, and introducing more when required by the data. An empirical approach is preferable to the use of a specific model in this case as it affords transparency concerning the correlations of galaxy and halo properties responsible for particular aspects of the predictions, provides model-independent information about the galaxy–halo connection, and ensures tight enough control over the model systematics for statistical tests to be meaningful. By comparing the predicted and observed MDARs we will deduce the extent to which semi-empirical models are able to account for the significant features of the relation, and the concrete extensions to basic models that are required to match the relation’s more detailed features. We intend in this way to lay the groundwork for a phenomenological determination of the galaxy–halo connection from information-rich relations such as the MDAR, as well as formulating precise tests for specific models.

The starting point of our framework is the technique of halo abundance matching (AM), which imposes a nearly monotonic relationship between galaxy stellar mass and halo mass or velocity at a particular epoch (Kravtsov et al. 2004; Conroy et al. 2006; Behroozi et al. 2010; Guo et al. 2010; Moster et al. 2010). Mocks based on AM have been shown to agree well with clustering and satellite fraction measurements (Reddick et al. 2013; Hearin et al. 2014; Lehmann et al. 2015), and, at least to first order, with 1-point galaxy scaling relations (Trujillo-Gomez et al. 2011; Desmond & Wechsler 2015, 2016). From a phenomenological perspective, AM specifies the relation between stellar mass and halo mass

and concentration required to fit observations, but in its basic form neglects gas mass as well as galaxy size and type. We therefore augment the model by allowing correlations of these variables with M_{vir} and c at fixed M_* . For a given set of correlations constituting the galaxy–halo connection, we generate a large number of mock data sets from our theoretical population with baryonic properties identical to the real data and halo properties specified by the model. We then calculate the MDAR statistics of these mock data sets, and evaluate the models by asking whether the observed values of the statistics could plausibly have been drawn from the mock data distributions.

The MDAR is considered by some an important piece of evidence in favour of Modified Newtonian Dynamics (MOND) as an alternative to Λ CDM for solving the missing mass problem, and is a central relation in MOND phenomenology (see Famaey & McGaugh 2012 and references therein). Indeed, the founding papers of MOND were the first to predict that \mathcal{D} would be more tightly correlated with acceleration than velocity or galactocentric radius (Milgrom 1983a,b,c), a hypothesis not verified empirically for many years. In MOND, the MDAR is a direct manifestation of the breakdown of Newtonian gravity or mechanics at low acceleration $a < a_0 \approx 1.2 \times 10^{-10} \text{ m s}^{-2}$, with the result that it is predicted to have no intrinsic scatter, residuals systematically uncorrelated with any other variable, and a clear acceleration scale $a = a_0$. While the MOND MDAR must go to 1 at $a \gg a_0$ (the Newtonian regime) and has a shape fixed by the theory at $a \ll a_0$ (the deep-MOND regime), the behaviour at intermediate a is specified by an *ad hoc* interpolating function. Our statistical analysis will shed light on the compatibility of the observations with the MOND hypothesis, and our comparison with Λ CDM models will bring into sharper focus the relative evidence accorded to MOND and Λ CDM by the relation.

The structure of this paper is as follows. In Section 2 we describe our observational MDAR sample and the N-body simulations on which we build our theoretical framework. In Section 3 we lay out our procedure for constructing the galaxy–halo connection and document the MDAR statistics with which we evaluate our models. In Section 4 we present our comparison of theory and data, first for a fiducial model best motivated by prior analyses, and then allowing variations in our model assumptions to maximise agreement with the MDAR. Section 5 discusses previous MDAR studies in the context of our results, locates our parameter constraints and model requirements relative to previous findings, and elaborates on the broader implications for our understanding of galaxy astrophysics. Section 6 concludes.

2 OBSERVED AND SIMULATED DATA

We take the observational MDAR from the SPARC sample (Lelli et al. 2016b),¹ a recent compilation of ~ 175 high-quality resolved rotation curves augmented with Spitzer 3.6 μm photometry. This sample spans a wide range in all dynamically-relevant galaxy properties ($6.7 < \log(M_*/M_\odot) < 11.4$, $0.18 < R_{\text{d}}/\text{kpc} < 18.8$, $7.2 < \log(M_{\text{gas}}/M_\odot) < 10.7$, and Hubble type S0 to Im/BCD), making it ideal for our analysis. Following the suggestion of Lelli et al. (2016b), we remove galaxies with quality flag $Q = 3$ (indicating major asymmetries, non-circular motions, and/or offsets between the stellar and HI distributions) and those with inclination $i < 30$ degrees, which may be subject to large systematic uncertainties in their rotation curves. We take $M_{\text{gas}} = 1.33 M_{\text{HI}}$ to account for molecular hydrogen, and adopt a stellar mass-to-light ratio of 0.5 (Lelli et al. 2016b). The MDAR of the final sample of 153 galaxies is shown in Figure 1.

Our theoretical framework is based on dark matter haloes from a simulation in the DARKSKY simulation suite (Skillman et al. 2014). The DARKSKY suite² assumes a flat Λ CDM cosmology with $h = 0.688$, $\Omega_m = 0.295$, $n_s = 0.968$, and $\sigma_8 = 0.834$. Here we use the DARKSKY-400 simulation (ds14_i_4096), a $(400 \text{ Mpc h}^{-1})^3$ box with 4096^3 particles and mass resolution $7.63 \times 10^7 h^{-1} M_\odot$, run with the 2HOT code (Warren 2013). This simulation was previously used in the studies of Lehmann et al. (2015), Desmond & Wechsler (2016), and Jennings et al. (2016). Haloes were identified using the ROCKSTAR halo finder (Behroozi, Wechsler & Wu 2013), and a merger tree was constructed using the CONSISTENT TREES code (Behroozi et al. 2013).

3 METHOD

We construct a series of empirical models of increasing complexity for the effective galaxy–halo connection of the SPARC sample. We begin with the standard AM ansatz that the only galaxy property that correlates with halo mass and concentration is stellar mass. We then consider the possibility that the SPARC galaxies inhabit a systematically biased subset of the total halo population, the potential for correlation between halo concentration and galaxy size at fixed stellar mass, and finally the impact of disk formation on the halo density profile. To test the models we use them to generate a large number of mock MDAR data sets with galaxy properties identical to the real data, but halo properties specified by the model. For each mock data set, we calculate a series of statistics based on important features of the MDAR, which we then compare to the values derived from the real data. We describe our theoretical framework in Section 3.1 and

¹ astroweb.cwru.edu/SPARC/

² darksky.slac.stanford.edu/

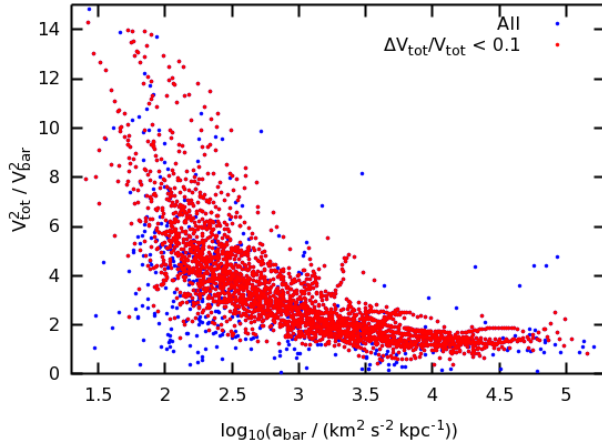


Figure 1. The mass discrepancy–acceleration relation of the high-quality subset of the SPARC data. 153 galaxies are included with an average of 21 measurement points for each. The highest precision points, which are likely to be least affected by non-circular motions, are shown in red.

our statistical analysis of the MDAR in Section 3.2. For quick reference, the free parameters of the framework are listed in Table 1, and the MDAR statistics in Table 2.

3.1 Model

We begin by assigning to the i^{th} galaxy in a given mock data set the observed stellar mass M_* and disc scale length R_d of the i^{th} SPARC galaxy. We perturb the observed stellar mass by the measurement uncertainty for that galaxy to estimate its true stellar mass. We then use AM to determine the set of DARKSKY-400 haloes that may host a galaxy of that stellar mass. To allow the most general dependence of stellar mass on halo mass and concentration, we use the AM parametrisation of Lehmann et al. (2015) in which the proxy is specified by a continuous free parameter, α :

$$\int_{M_*}^{\infty} \phi(M'_*) dM'_* = \int_{v_\alpha}^{\infty} n(v'_\alpha) dv'_\alpha, \quad (1)$$

where ϕ denotes galaxy number density per unit M_* , n denotes halo number density per unit v_α , and

$$v_\alpha \equiv v_{\text{vir}} \left(\frac{v_{\text{max}}}{v_{\text{vir}}} \right)^\alpha \quad (2)$$

evaluated at the epoch of peak halo mass. We allow also for a universal Gaussian scatter between M_* and v_α , which we term the AM scatter. By matching to luminosity and comparing AM mocks to clustering and satellite fraction measurements, Lehmann et al. (2015) find $\alpha = 0.6 \pm 0.2$ and AM scatter = 0.16 ± 0.04 , which we con-

sider as priors on our analysis. Our stellar mass function will be the single-Sersic fit of Bernardi et al. (2013).^{3,4}

We now select from the AM catalogue a halo mass and concentration for the i^{th} galaxy in the mock data set, by one of three methods.

(i) In the simplest method, we randomly select a halo from the stellar mass bin of the galaxy in question.⁵ This assumes no restriction on the type of halo that a SPARC galaxy may occupy.

(ii) Alternatively, we suppose that, due to their morphology or other properties, the SPARC galaxies inhabit a subset of the DARKSKY-400 haloes that is systematically offset from the mean in dynamically-relevant variables. This could obtain for example if late-type galaxies tend to inhabit less massive or less concentrated haloes than early-types, as suggested by Wojtak & Mamon (2013), Desmond & Wechsler (2015) and Mandelbaum et al. (2016) among others. To model this effect, we remove some fraction f of the highest concentration⁶ haloes at each stellar mass, and randomly select a halo from the remainder:

$$\frac{N_i(c > c_{\text{max},i})}{N_{\text{tot},i}} = f \quad (3)$$

for stellar mass bin i . A larger fraction corresponds to a stronger selection effect for the SPARC sample.

(iii) Finally, we consider the possibility that galaxy variables besides M_* are relevant for determining the type of halo to which a galaxy belongs. The “second parameter” most commonly considered in the literature is

³ Due to differences in photometric reductions, mass-to-light ratios or choice of IMF, the stellar masses we use for abundance matching may not be fully consistent with those of the SPARC data. A mismatch would imply that a given SPARC galaxy would be given a slightly incorrect halo mass, although this effect is largely degenerate with α . We discuss this issue further in Section 5.3.

⁴ The faint end of the SPARC sample, $M_* \approx 10^{6.7} M_\odot$, not only probes a region of the halo mass function where haloes may be poorly resolved in the DARKSKY-400 simulation, but also requires an uncertain extrapolation of the Bernardi et al. (2013) stellar mass function that we use for AM. We consider the benefits of a large stellar mass range to outweigh potential systematic errors from these effects, and hence do not cut the sample at the resolution limit. We caution however that results at the low-mass end may change as simulations acquire better resolution and galaxy surveys greater depth.

⁵ Wherever binning in M_* is required, we take 50 uniform bins in the range $6.7 < \log(M_*/M_\odot) < 11.4$.

⁶ M_{vir} could equally well be used as the two are largely degenerate in their effect on \mathcal{D} . We choose to use concentration because the stronger correlation between v_α and M_{vir} in our AM model causes c to have a larger spread at fixed M_* . In addition, we will see that the fiducial model places too much dark matter at small r , a problem more efficiently remedied by selecting on c than M_{vir} .

α	Interpolates AM proxy between M_{vir} ($\alpha = 0$) and v_{max} ($\alpha = 1$)
AM scatter	Universal Gaussian scatter in stellar mass at fixed proxy
f	Fraction of high-concentration haloes removed at fixed M_*
m	Slope of galaxy size–halo concentration correlation at fixed M_*
ν	Controls the degree of halo expansion (-) or contraction (+)

Table 1. Free parameters of the framework.

colour (e.g. Rodríguez-Puebla et al. 2011; Hearn & Watson 2013; Hearn et al. 2014), but for our purposes the most important variable neglected by AM is galaxy size, as quantified by R_{d} . This varies over two orders of magnitude in the SPARC sample and has a significant direct effect on a galaxy’s kinematics and hence its position on the MDAR. Not only is there no reason for a correlation between R_{d} and c at fixed M_* not to exist, but in fact it is motivated both by its presence in the angular momentum-based galaxy formation model of Mo, Mao & White (1998) and by the suggestion of Desmond & Wechsler (2016) that such a correlation may be required to match the small scatter of the Fundamental Plane. To capture the leading order effect of this relation on the MDAR, we introduce a toy model for correlating the radius residuals of the $M_* - R_{\text{d}}$ relation with the concentration residuals of the $M_* - c$ relation. We assert that on average the concentration residual is a fixed multiple m of the radius residual, with a fiducial 0.1 dex Gaussian scatter:

$$\Delta c \sim \mathcal{N}(m \cdot \Delta R_{\text{d}}, 0.1), \quad (4)$$

where

$$\Delta x \equiv \log(x) - \langle \log(x) | M_* \rangle. \quad (5)$$

When $m < 0$, larger galaxies tend to live in less concentrated haloes (in accordance with Mo et al. 1998), and vice-versa for $m > 0$. This will this allow us to test for such a correlation in the MDAR data and absorb any discrepancies that may be related to the galaxy–halo connection in this way. When using this method, we first determine c from M_* and R_{d} , and then randomly select M_{vir} from the subset of the AM-matched catalogue at this M_* and c .

We have now associated a halo with each SPARC galaxy in a given mock data set; it remains to lay out the baryonic and dark matter mass profiles and determine a and \mathcal{D} along the rotation curve. We consider at this stage the impact of disk formation on the halo density distribution. While pristine dark matter haloes have a density profile well-characterised by the NFW form, galaxy formation draws dark matter inwards by adiabatic contraction (Blumenthal et al. 1986; Gnedin et al. 2004, 2011), and may subsequently move it outwards again through stellar feedback (e.g. Mashchenko et al. 2008; Governato

et al. 2010; Pontzen & Governato 2012). Following Dutton et al. (2007) and Desmond & Wechsler (2015, 2016), we parameterize these effects by means of a single free parameter ν , which interpolates between the adiabatic contraction model of Gnedin et al. (2011) ($\nu = 1$) and an expansion of the same magnitude ($\nu = -1$).⁷ We take our fiducial value of ν to be -0.5 , which has been shown to produce agreement with the normalisation of the Tully–Fisher and Faber–Jackson relations (Dutton et al. 2013; Desmond & Wechsler 2015, 2016). Although this parametrisation must capture the leading order effect of halo expansion or contraction, we caution that in the absence of consensus concerning the effect of feedback on galaxy formation its precise mass and radius dependence remains somewhat arbitrary. We will discuss this issue further in Section 5.3. ν is the fifth and final free parameter of our framework.

This prescription for halo contraction or expansion requires as input the full baryonic mass distribution of a model galaxy. To estimate this, we assume that each galaxy is composed of a bulge, a thin exponential stellar disk, and a thin exponential gas disk. We take the bulge mass fraction, gas mass and stellar disk scale length directly from the SPARC data on a galaxy-by-galaxy basis (the first by personal communication, F. Lelli), and calculate the gas disk scale length $R_{\text{d,gas}}$ from the measured radius (RHI) at which the HI surface density drops below $1 M_{\odot}/\text{pc}^2$.⁸ For a given value of ν , and for a given abundance-matched galaxy, this enables us to determine the full dark matter mass profile $M_{\text{DM}}(< r)$.

We are now in position to derive the MDAR of each mock data set. To do this, we calculate for the i^{th} mock galaxy the enclosed halo mass within each of the radii actually sampled for the i^{th} SPARC galaxy, and hence V_{DM}^2 . We take the baryonic contribution V_{bar}^2 to be exactly as calculated for the real data, and hence determine the to-

⁷ In some feedback models, dark matter is moved outwards only in the inner regions of galaxies, and continues to move in by adiabatic contraction further out. Since $\nu < 0$ implies halo expansion at all radii, it may underestimate the amount of dark matter at intermediate to large radii relative to such models.

⁸ For some galaxies in which the gas profile is far from exponential it is not possible to derive a self-consistent value for $R_{\text{d,gas}}$. In these cases we take the value closest to providing a solution. For galaxies in which RHI was not measured, we use $R_{\text{d,gas}} = 2R_{\text{d}}$ (Lelli et al. 2016b).

tal velocity $V^2 = V_{\text{bar}}^2 + V_{\text{DM}}^2$. Since this is the “true” model velocity while the data uses the observed velocity, we scatter it by the median quoted measurement uncertainty (7 per cent) before calculating the mass discrepancy $\mathcal{D}(r) = (V_{\text{bar}}^2(r) + V_{\text{DM}}^2(r))/V_{\text{bar}}^2(r)$. We cast the MDAR in terms of the baryonic acceleration $a_{\text{bar}} = V_{\text{bar}}^2/r$ rather than the total acceleration $a_{\text{tot}} = V_{\text{tot}}^2/r$ so that the values of the independent variables in the mock and real data sets are identical. For convenience, we use the definition $a \equiv \log(a_{\text{bar}}/(\text{km}^2 \text{ s}^{-2} \text{ kpc}^{-1}))$ hereafter. Note that we do *not* use the above bulge-disk decompositions of the baryon mass profile in the calculation of V_{bar}^2 : these are approximate and required only for implementing our halo expansion/contraction scheme.⁹ Using identical V_{bar} values for the mock and real data sets ensures that any difference in their MDARs is due to the dark matter distribution, and are therefore attributable to the galaxy–halo connection.

By compiling the $a - \mathcal{D}$ curves for each of the 153 galaxies in a given mock data set, we produce a theoretical MDAR fully commensurable with that observed. We repeat this procedure 2000 times to generate an ensemble of mock MDAR data sets statistically representative of the underlying model, which we then subject to the following testing.

3.2 Statistical analysis and comparison of theory and observation

As discussed in Section 1, we wish to understand four aspects of the MDAR and their relation to theoretical expectations: shape, scatter, the presence of a “characteristic acceleration” beyond which mass discrepancies consistently go to ~ 1 , and the correlation of residuals with other galaxy properties. We devise a series of statistics to quantify these features, and compare the observed values to the distributions obtained from Monte Carlo realisations of the models. In determining appropriate statistics, it is important to consider the level of detail at which one wishes to probe the relation. We cannot expect the model to match statistics that reflect finer-grained aspects of the relation than we can reasonably hope it to predict, but on the other hand statistics not fine enough may imply agreement where in detail there is none. In addition, we consider statistics explicitly tied to physically meaningful features of the MDAR to be more useful than those giving simply an overall measure of agreement, since they provide a concrete idea of how to improve the model.

We propose the following. (i)–(v) relate to the shape and scatter of the MDAR, (vi)–(ix) to the presence of a

⁹ The fact that the baryonic mass profile implied by the measured V_{bar}^2 is not equivalent to the bulge-disk decomposition introduces a small error into $M_{\text{DM}}(< r)$ for given ν . Since halo expansion is a second-order effect in the final MDAR, and variations in the baryonic mass distribution are in any case largely degenerate with ν , this is permissible.

“characteristic acceleration scale,” and (x) to the correlation of MDAR residuals with other galaxy properties. The statistics are summarised in Table 2.

(i)

$$\langle \mathcal{D} \rangle_1 \equiv \frac{\sum_{a=1.5}^{1.66} \mathcal{D}}{N(1.5, 1.66)}, \quad (6)$$

where $N(x, y)$ is the number of data points in the range $x < a < y$. This is the average¹⁰ \mathcal{D} in the first a bin,¹¹ and describes the relative amount of dark and baryonic matter in low acceleration regions.

(ii)

$$\langle \mathcal{D} \rangle_{16} \equiv \frac{\sum_{a=3.84}^4 \mathcal{D}}{N(3.84, 4)}, \quad (7)$$

the corresponding statistic for the last a bin. This statistic and the above give an indication of the shape of the MDAR.

(iii)

$$\sigma(\mathcal{D})_1 \equiv \left(\frac{\sum_{a=1.5}^{1.66} \mathcal{D}^2}{N(1.5, 1.66)} - \langle \mathcal{D} \rangle_1^2 \right)^{\frac{1}{2}}. \quad (8)$$

This measures the spread in \mathcal{D} in the first a bin and hence quantifies the effect of variations between galaxies at low acceleration.

(iv)

$$\sigma(\mathcal{D})_{16} \equiv \left(\frac{\sum_{a=3.84}^4 \mathcal{D}^2}{N(3.84, 4)} - \langle \mathcal{D} \rangle_{16}^2 \right)^{\frac{1}{2}}, \quad (9)$$

the corresponding statistic for the last a bin.

(v)

$$\sigma_{\text{tot}}^2 \equiv \frac{\sum_{i=1}^{16} \sigma(\mathcal{D})_i^2 \cdot N(a_i, a_{i+1})}{N(1.5, 4)}, \quad (10)$$

where i is the bin index and a_i is the lower limit of bin i . This is the average variance in \mathcal{D} over all the a bins, weighted by the number of points in each bin. σ_{tot}^2 measures the overall scatter of the MDAR.

(vi)

$$\langle \mathbf{a} \rangle \equiv \frac{\sum_{j=1}^{N_{\text{cross}}} \mathbf{a}_j}{N_{\text{cross}}}, \quad (11)$$

where \mathbf{a}_j is the a value at which galaxy j crosses $\mathcal{D} = 3$,¹² and $N_{\text{cross}} = 153 - \mathcal{F}_+ - \mathcal{F}_-$ is the number of galaxies

¹⁰ Unless otherwise stated, all averages are means.

¹¹ Where binning in acceleration is required, we use 16 bins uniformly spaced in the range $1.5 < a < 4$. The first and last bins therefore occupy the ranges $1.5 < a < 1.66$ and $3.84 < a < 4$ respectively.

¹² We choose a threshold value of 3 because this minimises $\mathcal{F}_+ + \mathcal{F}_-$ in the data (see below), and hence maximises the number of galaxies for which \mathbf{a} is defined. Raising the threshold increases \mathcal{F}_- and decreases \mathcal{F}_+ , and vice versa. Moderate perturbations to the threshold value (± 1) do not significantly

$\langle \mathcal{D} \rangle_1$	Average \mathcal{D} in range $1.5 < a < 1.66$
$\langle \mathcal{D} \rangle_{16}$	Average \mathcal{D} in range $3.84 < a < 4$
$\sigma(\mathcal{D})_1$	Standard deviation in \mathcal{D} over range $1.5 < a < 1.66$
$\sigma(\mathcal{D})_{16}$	Standard deviation in \mathcal{D} over range $3.84 < a < 4$
σ_{tot}^2	Weighted average variance in \mathcal{D} over range $1.5 < a < 4$
$\langle \mathfrak{a} \rangle$	Average value of a at which \mathcal{D} drops below 3
$\sigma(\mathfrak{a})$	Standard deviation in value of a at which \mathcal{D} drops below 3
\mathcal{F}_+	Number of galaxies with $\mathcal{D} > 3$ across their rotation curve
\mathcal{F}_-	Number of galaxies with $\mathcal{D} < 3$ across their rotation curve
$\langle \Delta(\mathcal{D})_{M_*} \rangle$	Weighted average difference in \mathcal{D} between high and low M_* galaxies at fixed a
$\langle \Delta(\mathcal{D})_{\Delta R_d} \rangle$	Weighted average difference in \mathcal{D} between large and small galaxies at fixed M_* and a
$\langle \Delta(\mathcal{D})_{\Delta M_{\text{gas}}} \rangle$	Weighted average difference in \mathcal{D} between high and low M_{gas} galaxies at fixed M_* and a
$\langle \Delta(\mathcal{D})_T \rangle$	Weighted average difference in \mathcal{D} between late and early type galaxies at fixed a
$\langle \Delta(\mathcal{D})_r \rangle$	Weighted average difference in \mathcal{D} between high and low sampling radii at fixed a

Table 2. MDAR diagnostic statistics. Rows 1-5 measure the shape and scatter of the MDAR, rows 6-9 quantify the relation’s “acceleration scale,” and rows 10-14 assess the dependence of \mathcal{D} on various dynamically-relevant galaxy properties at fixed a . For the full definitions, see Eqs. 6–14.

within this data set for which this happens (see below). \mathfrak{a}_j is a proxy for the acceleration at which dark matter becomes dynamically negligible in galaxy j , and hence $\langle \mathfrak{a} \rangle$ indicates the “characteristic acceleration scale” of this data set. Note that in a given data set not all galaxies have some measured points at $\mathcal{D} > 3$ and some at $\mathcal{D} < 3$; for galaxies that do not \mathfrak{a} is undefined. The number of such galaxies is measured by \mathcal{F}_+ and \mathcal{F}_- , below.

(vii)

$$\sigma(\mathfrak{a}) \equiv \left(\frac{\sum_{j=1}^{N_{\text{cross}}} \mathfrak{a}_j^2}{N_{\text{cross}}} - \langle \mathfrak{a} \rangle^2 \right)^{\frac{1}{2}}. \quad (12)$$

The spread in \mathfrak{a} values among galaxies measures the similarity of the “acceleration scales” of different galaxies within a data set. The smaller $\sigma(\mathfrak{a})$, the more unique this scale and hence the more it may be said to be “characteristic.”

(viii) \mathcal{F}_+ , the number of galaxies with $\mathcal{D} > 3$ across their rotation curve. These galaxies do not possess a value for \mathfrak{a} and are therefore excluded in the calculation of $\langle \mathfrak{a} \rangle$ and $\sigma(\mathfrak{a})$ above.

(ix) \mathcal{F}_- , the number of galaxies with $\mathcal{D} < 3$ across their rotation curve. As above.¹³

(x)

$$\langle \Delta(\mathcal{D})_X \rangle \equiv \quad (13)$$

$$\frac{\sum_{i=1}^{16} (\langle \mathcal{D} \rangle_{i;X_2} - \langle \mathcal{D} \rangle_{i;X_1}) \cdot \min(N_{X_1}(a_i, a_{i+1}), N_{X_2}(a_i, a_{i+1}))}{\sum_{i=1}^{16} \min(N_{X_1}(a_i, a_{i+1}), N_{X_2}(a_i, a_{i+1}))},$$

affect the results. To calculate \mathfrak{a} , we linearly interpolate between the two measured accelerations on either side of $\mathcal{D} = 3$.¹³ Note that a fair comparison of \mathcal{F}_+ and \mathcal{F}_- between mock and real data sets requires that the rotation curves be sampled at identical radii for each. Analysis at this level of detail could not therefore be performed using the method of van den Bosch & Dalcanton (2000) or Di Cintio & Lelli (2016), for example.

where

$$X = \{M_*, \Delta R_d, \Delta M_{\text{gas}}, T, r\}, \quad (14)$$

Δx is defined in Eq. 5, X_1 labels points at low X , and X_2 at high X . For $X = \{M_*, \Delta R_d, \Delta M_{\text{gas}}\}$, X_1 corresponds to galaxies with X in the bottom third of the SPARC sample, and X_2 to galaxies in the upper third. For $X = r$, X_1 corresponds to the third of measurement points taken at lowest galactocentric radius (separately for each galaxy), and X_2 to the corresponding upper third. For $X = T$, X_1 denotes galaxies with Hubble type S0–Sb (27 galaxies), and X_2 those with type Sd–Sdm (26 galaxies). We weight by $\min(N_{X_1}(a_i, a_{i+1}), N_{X_2}(a_i, a_{i+1}))$ in order to prioritise the bins with the lowest shot noise, which contain many points from both subsamples.

These statistics measure the average vertical offset between the MDARs at low and high X . An offset significantly different from 0 would imply that the MDAR is dependent on X , and *a fortiori* that \mathcal{D} is not a function of a alone. The values of X we consider here are the dynamically-relevant galaxy properties that may be expected to influence the MDAR in a generic theory of galaxy formation. In particular, by comparing the predicted and observed $\langle \Delta(\mathcal{D})_X \rangle$ we can hope to get a handle on the following: the dynamical validity of the AM stellar mass–halo mass relation ($X = M_*$), the correlation of galaxy size with halo properties at fixed stellar mass ($X = \Delta R_d$), the validity of the assumption that the halo proxy in AM is uncorrelated with cold gas mass at fixed stellar mass ($X = \Delta M_{\text{gas}}$), the relation between galaxy morphology and halo properties ($X = T$), and finally the radius dependence of the halo density distribution ($X = r$).

Associated with each statistic for a given model is a two-tailed p -value equal to the fraction of mock data sets with a more extreme value for that statistic than the

data. We will say that a model fails to account for statistic j (and hence the associated feature of the MDAR) if a value of j at least as extreme as the real data's has a $p < 0.05$ probability of being randomly drawn from the mock data distribution.

4 RESULTS

4.1 Fiducial model

We begin with a fiducial model in which α , AM scatter and ν are chosen in accordance with the results of previous AM studies (0.6, 0.16 and -0.5 respectively; Lehmann et al. 2015; Desmond & Wechsler 2015, 2016), and f and m are set to 0. This is the maximum-likelihood prior expectation for the description of the galaxy–halo connection by AM, assuming no dependence of galaxy size or type on halo properties. The results are shown in Tables 3–5 (second row) and Figs. 2–7 (in red where models are compared).

The columns in Tables 3–5 corresponds to the statistics described in Section 3.2; those pertaining to MDAR shape and scatter are shown in Table 3, characteristic acceleration in Table 4, and the correlation of MDAR residuals in Tables 5. The first row lists the values in the real data, while subsequent rows contain the results for various models. In these cases, we give the modal average value of the statistic over all the Monte Carlo mock data sets, as well as the upper and lower limits enclosing 95 per cent of the results. If the value in the data lies outside these limits (and assuming negligible systematic error), then the null hypothesis that the data was drawn from the model may be rejected at the 95 per cent confidence level, according to that statistic.

Fig. 2 compares the real data in blue to a stack of 2000 Monte Carlo realisations of the theoretical galaxy population in magenta and a randomly-chosen example mock data set in green. Fig. 3(a) shows the average mass discrepancy in each bin of acceleration, $\langle \mathcal{D} \rangle_i$, averaged over all mock data sets (thick line) with the associated 2σ scatter between mock data sets (thin lines); Fig. 3(b) is the analogue for the standard deviations $\sigma(\mathcal{D})_i$. Fig. 4 compares the weighted average variance in \mathcal{D} , σ_{tot}^2 , for the mock and real data. Fig. 5 is a normalised histogram of \mathbf{a} for the real galaxies (red), and the mock galaxies stacked over all Monte Carlo realisations (blue). The insets show the distributions of \mathcal{F}_+ and \mathcal{F}_- over the mock data sets, compared to the corresponding values for the real data. Figs. 6(a) and 6(b) plot the distributions of $\langle \mathbf{a} \rangle$ and $\sigma(\mathbf{a})$ respectively. Finally, Fig. 7 shows the average offset $\langle \Delta(\mathcal{D})_x \rangle$ in \mathcal{D} between subsets of the data split by M_* , ΔR_{d} , ΔM_{gas} , T , and r .

The results are as follows.

(i) A visual inspection of Fig. 2 reveals that the shape of the observed MDAR roughly traces the model expectation. \mathcal{D} is low at high a (where baryons dominate),

and dark matter becomes increasingly important towards lower a . This result is known from the work of van den Bosch & Dalcanton (2000) and Di Cintio & Lelli (2016).

(ii) However, it is also evident from Fig. 2 that both $\langle \mathcal{D} \rangle$ and $\sigma(\mathcal{D})$ are too high at low a ; that is, there exists an excess of dark matter in low acceleration regions, in addition to excessive scatter between galaxies. In a given realisation of the model, several measured points would be expected at $\mathcal{D} > 25$, while none are observed. These results are confirmed in Fig. 3, and the 3rd and 5th columns of Table 3, where it is shown that the discrepancy in the first a bin is 5.5σ in $\langle \mathcal{D} \rangle$ and 2.3σ in $\sigma(\mathcal{D})$. The discrepancy in the weighted average variance, σ_{tot}^2 , is 3.6σ .

(iii) A crossover occurs at $a \sim 2.8$, beyond which the simulated measurements lie below the observations in both $\langle \mathcal{D} \rangle$ and $\sigma(\mathcal{D})$. This shows that standard AM (with moderate halo expansion) readily accounts for the baryon-domination of high-acceleration regions, and furthermore that variations in the dark matter content among galaxies at high a are naturally small. In fact, it is seen from the 4th and 6th columns of Table 3 that the predicted $\langle \mathcal{D} \rangle$ and $\sigma(\mathcal{D})$ are both $> 4\sigma$ too *low* in the 16th bin, which implies at face value that high-acceleration regions ought to possess more dark matter than allowed for by our fiducial model. Although the quoted measurement uncertainties in the SPARC data ($\lesssim 15$ per cent in V_{tot}) are too small to reconcile the measured values with the theoretical expectations, there exist additional uncertainties due to disc inclination, mass-to-light ratio, distance, and three dimensional baryon structure (personal communication, F. Lelli). Taken together, these could account for the discrepancy in $\langle \mathcal{D} \rangle_{16}$ and $\sigma(\mathcal{D})_{16}$, but would exacerbate the overprediction of $\sigma(\mathcal{D})_1$ and σ_{tot}^2 .

(iv) When the line traced by a galaxy in the $a - \mathcal{D}$ plane crosses $\mathcal{D} = 3$, it does so at an acceleration \mathbf{a} in the range $2.3 \lesssim a \lesssim 3.3$. The distribution of \mathbf{a} values over all galaxies in a mock data set is comparable to that of the real data, although typically centred on a slightly higher value (Figs. 5(a) and 6(a), and column 3 of Table 4). Remarkably, the spread in \mathbf{a} , $\sigma(\mathbf{a})$, is actually *lower* in the model than in the data (Fig. 6(b) and column 4 of Table 4), indicating a *greater* degree of regularity in the acceleration beyond which dark matter becomes dynamically irrelevant. These results imply that if the real galaxies are said to exhibit a “characteristic acceleration,” so too should the model galaxies.

(v) However, only a fraction of the galaxies in each data set have points on either side of $\mathcal{D} = 3$. Some have $\mathcal{D} > 3$ at all observed points along their rotation curve (typically low surface brightness galaxies that are dark matter-dominated even near the centre) and hence contribute to \mathcal{F}_+ , while others have $\mathcal{D} < 3$ everywhere (typically those with insufficient gas to probe the outer low- a regions) and hence contribute to \mathcal{F}_- . We see from the inset of Fig. 5(a), as well as columns 5 and 6 of Table 4, that many more mock galaxies have $\mathcal{D} > 3$ than ob-

Model	$(\alpha, \text{AM scatter}, f, m, \nu)$	$\langle \mathcal{D} \rangle_1$	$\langle \mathcal{D} \rangle_{16}$	$\sigma(\mathcal{D})_1$	$\sigma(\mathcal{D})_{16}$	σ_{tot}^2
SPARC data	—	11.4	1.54	7.74	0.375	2.88
Fiducial	0.6, 0.16, 0, 0, -0.5	24.9^{+8.8}_{-4.9}	$1.20^{+0.11}_{-0.05}$	17.5^{+17.1}_{-8.5}	$0.18^{+0.09}_{-0.04}$	19.7^{+34.6}_{-9.4}
No AM scatter	0.6, 0, 0, 0, -0.5	24.6^{+9.4}_{-5.1}	$1.25^{+0.07}_{-0.09}$	19.0^{+16.1}_{-11.1}	$0.20^{+0.08}_{-0.05}$	21.0^{+28.1}_{-12.5}
Strong halo expansion	0.6, 0.16, 0, 0, -1	24.3^{+8.0}_{-5.8}	$1.14^{+0.07}_{-0.06}$	14.5^{+19.5}_{-6.2}	$0.18^{+0.06}_{-0.04}$	22.9^{+23.0}_{-13.5}
Adiabatic contraction	0.6, 0.16, 0, 0, 1	30.4^{+9.2}_{-5.4}	1.97^{+0.21}_{-0.16}	21.3^{+18.5}_{-9.3}	0.87^{+0.52}_{-0.34}	31.2^{+28.2}_{-13.1}
Strong concentration selection	0.6, 0.16, 0.8, 0, -0.5	$13.5^{+2.1}_{-2.6}$	$1.09^{+0.04}_{-0.04}$	$4.03^{+4.50}_{-1.21}$	$0.15^{+0.03}_{-0.02}$	$2.87^{+4.72}_{-1.57}$
Distinct haloes only	0.6, 0.16, 0, 0, -0.5	22.5^{+6.3}_{-3.9}	$1.20^{+0.08}_{-0.07}$	13.6^{+8.3}_{-6.6}	$0.19^{+0.05}_{-0.04}$	11.3^{+13.3}_{-4.9}
$\Delta R_d - \Delta c$ anticorrelation	0.6, 0.16, 0, -0.3, -0.5	24.8^{+3.9}_{-3.7}	$1.23^{+0.09}_{-0.06}$	$11.4^{+3.7}_{-3.3}$	$0.19^{+0.05}_{-0.03}$	9.00^{+2.37}_{-3.39}

Table 3. Statistics pertaining to the shape and scatter of the MDAR in the data (first row), and under various model assumptions (remaining rows). The numbers quoted for the models are modal averages across 2000 Monte Carlo realisations, along with the minimal bounds enclosing 95 per cent of the realisations. Bold indicates a prediction that we argue demonstrates a problem with the corresponding model, or motivates an alternative. See also Figs. 3 and 4.

Model	$(\alpha, \text{AM scatter}, f, m, \nu)$	$\langle \mathbf{a} \rangle$	$\sigma(\mathbf{a})$	\mathcal{F}_+	\mathcal{F}_-
SPARC data	—	2.66	0.313	46	26
Fiducial	0.6, 0.16, 0, 0, -0.5	$2.82^{+0.08}_{-0.04}$	$0.24^{+0.05}_{-0.05}$	87^{+5}_{-5}	10^{+4}_{-4}
No AM scatter	0.6, 0, 0, 0, -0.5	$2.85^{+0.07}_{-0.05}$	$0.25^{+0.04}_{-0.06}$	87^{+5}_{-5}	10^{+3}_{-4}
Strong halo expansion	0.6, 0.16, 0, 0, -1	$2.77^{+0.07}_{-0.05}$	$0.25^{+0.06}_{-0.05}$	81^{+5}_{-5}	12^{+5}_{-4}
Adiabatic contraction	0.6, 0.16, 0, 0, 1	3.14^{+0.09}_{-0.10}	$0.26^{+0.11}_{-0.05}$	117⁺⁴₋₅	4⁺³₋₃
Strong concentration selection	0.6, 0.16, 0.8, 0, -0.5	$2.57^{+0.05}_{-0.06}$	$0.20^{+0.05}_{-0.04}$	71^{+5}_{-5}	22^{+7}_{-6}
Distinct haloes only	0.6, 0.16, 0, 0, -0.5	$2.84^{+0.04}_{-0.08}$	$0.24^{+0.05}_{-0.04}$	85^{+5}_{-5}	8^{+4}_{-2}
$\Delta R_d - \Delta c$ anticorrelation	0.6, 0.16, 0, -0.3, -0.5	$2.91^{+0.04}_{-0.05}$	$0.19^{+0.04}_{-0.04}$	91^{+3}_{-5}	7^{+4}_{-2}

Table 4. Statistics pertaining to the “characteristic acceleration” of the MDAR in the data (first row), and under various model assumptions (remaining rows). The numbers quoted for the models are modal averages across 2000 Monte Carlo realisations, along with the minimal bounds enclosing 95 per cent of the realisations. Bold indicates a prediction that we argue demonstrates a problem with the corresponding model, or motivates an alternative. See also Figs. 5 and 6.

Model	$(\alpha, \text{AM scatter}, f, m, \nu)$	$\langle \Delta(\mathcal{D})_{M_*} \rangle$	$\langle \Delta(\mathcal{D})_{\Delta R_d} \rangle$	$\langle \Delta(\mathcal{D})_{\Delta M_{\text{gas}}} \rangle$	$\langle \Delta(\mathcal{D})_T \rangle$	$\langle \Delta(\mathcal{D})_r \rangle$
SPARC data	—	-0.574	-0.853	-0.317	-0.730	-0.297
Fiducial	0.6, 0.16, 0, 0, -0.5	$-1.33^{+2.01}_{-1.64}$	0.31^{+1.58}_{-1.44}	$-0.53^{+1.08}_{-1.03}$	$0.15^{+1.50}_{-1.56}$	-3.06^{+0.89}_{-1.58}
No AM scatter	0.6, 0, 0, 0, -0.5	$-1.04^{+1.74}_{-1.59}$	0.20^{+1.70}_{-1.28}	$-0.36^{+1.03}_{-1.49}$	$0.11^{+1.20}_{-1.26}$	-3.34^{+1.37}_{-1.19}
Strong halo expansion	0.6, 0.16, 0, 0, -1	$-1.19^{+2.23}_{-1.43}$	0.13^{+1.61}_{-1.22}	$-0.36^{+0.96}_{-1.12}$	$-0.25^{+1.73}_{-1.07}$	-2.66^{+1.23}_{-1.36}
Adiabatic contraction	0.6, 0.16, 0, 0, 1	$-1.94^{+1.71}_{-1.81}$	0.78^{+1.11}_{-2.01}	$-0.48^{+1.22}_{-0.87}$	$1.11^{+1.63}_{-1.40}$	-5.70^{+1.09}_{-1.35}
Strong concentration selection	0.6, 0.16, 0.8, 0, -0.5	$0.66^{+0.89}_{-1.16}$	0.15^{+0.73}_{-0.62}	$0.20^{+0.36}_{-0.53}$	$-0.55^{+0.99}_{-0.85}$	$-0.14^{+0.32}_{-0.43}$
Distinct haloes only	0.6, 0.16, 0, 0, -0.5	$-0.08^{+1.39}_{-1.55}$	0.58^{+1.05}_{-1.30}	$-0.11^{+0.76}_{-0.94}$	$-0.20^{+1.01}_{-1.44}$	-1.77^{+0.74}_{-0.98}
$\Delta R_d - \Delta c$ anticorrelation	0.6, 0.16, 0, -0.3, -0.5	$-0.91^{+1.36}_{-1.17}$	$-0.95^{+0.92}_{-0.79}$	-0.75^{+0.68}_{-0.56}	$-0.23^{+0.93}_{-1.17}$	-2.12^{+0.46}_{-0.65}

Table 5. Statistics pertaining to the dependence of the MDAR on various galaxy properties in the data (first row), and under various model assumptions (remaining rows). The numbers quoted for the models are modal averages across 2000 Monte Carlo realisations, along with the minimal bounds enclosing 95 per cent of the realisations. Bold indicates a prediction that we argue demonstrates a problem with the corresponding model, or motivates an alternative. See also Fig. 7.

served, but fewer have $\mathcal{D} > 3$. This is a consequence of the mismatch of the shape of the predicted and observed MDARs, which is manifest also in the fact that $\langle \mathcal{D} \rangle_1$ is too high and $\langle \mathcal{D} \rangle_{16}$ too low.

(vi) The observed values of $\langle \Delta(\mathcal{D})_{M_*} \rangle$, $\langle \Delta(\mathcal{D})_{\Delta M_{\text{gas}}} \rangle$ and $\langle \Delta(\mathcal{D})_T \rangle$ are compatible with the corresponding theoretical distributions (Figs. 7(a), 7(c) and 7(d) and 3rd, 5th and 6th columns of Table 5). This implies that the dependence of halo mass on stellar mass generated by AM is adequate, and that the MDAR does not favour a modification to stellar mass-based AM to include gas. That $\langle \Delta(\mathcal{D})_T \rangle$ is consistent between theory and data suggests that at fixed stellar mass, S0 and Sd galaxies do not live in haloes with significantly different mass or concentration.¹⁴ We note, however, that the large spread of $\langle \Delta(\mathcal{D})_X \rangle$ values in the mock data (due to the excessive scatter in \mathcal{D}) makes it difficult to draw definitive conclusions.¹⁵ We caution also that these results are sensitive to the free parameters of the model, an issue to which we will return in Section 4.2.

(vii) $\langle \Delta(\mathcal{D})_{\Delta R_d} \rangle$ is typically larger in the mock data than the real data (Fig. 7(b) and 4th column of Table 5). This implies that smaller galaxies at fixed stellar mass (i.e. those of higher surface brightness) live in more massive or more concentrated haloes than they have been assigned, and vice versa for larger galaxies. In Section 4.2 we will use a correlation between galaxy size and halo concentration to explore this issue further.

(viii) $\langle \Delta(\mathcal{D})_r \rangle$ is smaller in the mock data than the real data by around 6σ (Fig. 7(e) and 7th column of Table 5). This discrepancy – a relative of the well-known cusp/core problem for dwarf galaxies – indicates that too much dark matter resides in the inner regions of galaxies in the model. In Section 4.2 we will use this result as further evidence for the hypothesis that the SPARC galaxies must reside in a low-concentration subset of the total halo population if an AM-based model is to be able to account for the MDAR in detail.

(ix) The magnitudes of $\langle \Delta(\mathcal{D})_X \rangle$ in the data are all small (< 1). The average measurement uncertainty of 7 per cent in V_{tot} corresponds to a 14 per cent uncertainty in \mathcal{D} , which equates to $\Delta(\mathcal{D}) \approx 0.5$ when averaged

¹⁴ There is a hint that the mass discrepancies of the earlier-type galaxies in the SPARC sample need to be boosted relative to those of later type (i.e. the predicted $\langle \Delta(\mathcal{D})_T \rangle$ is too large). Although statistically insignificant, this offset is in the same direction as the indications from weak lensing and satellite kinematics (Rodríguez-Puebla et al. 2011; Wojtak & Mamon 2013; Mandelbaum et al. 2016).

¹⁵ Note that an independence of halo properties on type, size or gas mass at fixed stellar mass (as in the fiducial model) does not imply $\langle \Delta(\mathcal{D})_X \rangle = 0$. This statistic depends on the contingent details of the baryonic mass distributions and sampling radii of the SPARC galaxies. The only way to acquire information concerning these aspects of the galaxy–halo connection, therefore, is to compare mock and real data sets in which these distributions and radii are the same.

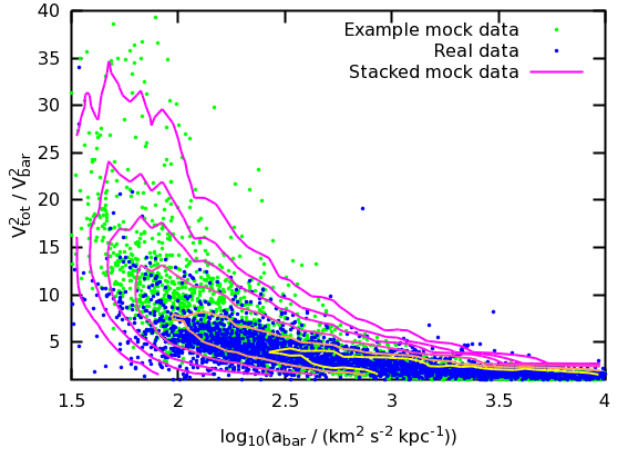


Figure 2. Comparison of the observed MDAR (blue points) to that predicted by the fiducial model (green points and contour). The contours enclose 40, 60, 80, 90, 95 and 98 per cent of mock data points from 2000 Monte Carlo realisations of the model, while the green points show an example realisation.

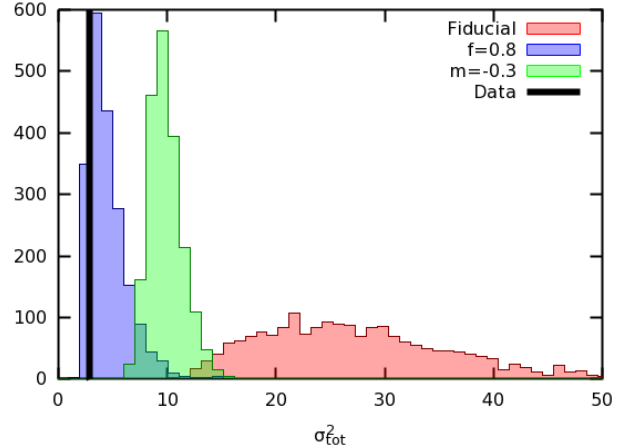


Figure 4. Distributions of the weighted average variance (σ_{tot}^2) in the MDAR for various model assumptions, compared to the value in the data. The red, blue and green histograms correspond to the 2nd, 7th and 8th rows in Tables 3–5 respectively. Only a strong selection on halo concentration can reduce the predicted σ_{tot}^2 to acceptable levels.

over the entire MDAR. Hence the systematic offset in the MDAR as each X is varied is small enough to be accounted for by measurement error alone, and \mathcal{D} is consistent with being a function only of a .

4.2 Variations to model parameters

We now investigate the effect of variations in the model parameters, with a particular eye to mitigating the dis-

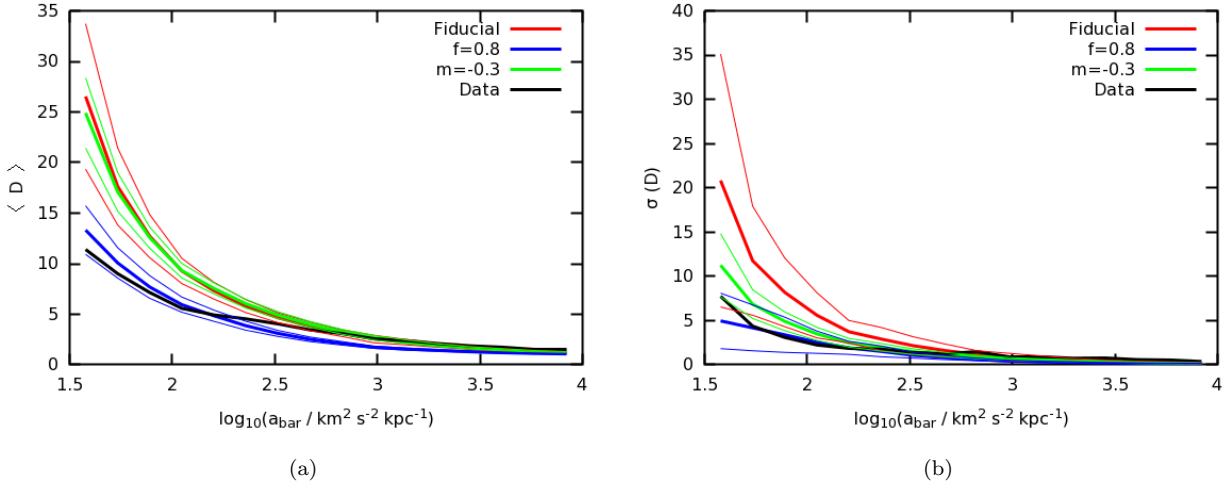


Figure 3. The average (thick lines) and 2σ scatter (thin lines) across 2000 mock data sets of the mean mass discrepancy ($\langle \mathcal{D} \rangle$; Fig. 3(a)) and its standard deviation ($\sigma(\mathcal{D})$; Fig. 3(b)) in 16 bins of acceleration, compared to the real data values. Models without strong concentration selection overpredict $\langle \mathcal{D} \rangle$ and $\sigma(\mathcal{D})$ at low a .

crepancies noted above. We first consider the possibility of reducing the predicted MDAR scatter by decreasing the AM scatter: the results of a model with AM scatter = 0 are shown in the 3rd row of Tables 3–5. This has a negligible effect on the statistics characterising the shape and scatter of the relation, indicating that $\sigma(\mathcal{D})$ originates almost entirely from the spread in \mathcal{D} values generated by haloes of fixed proxy (due to scatter in M_{vir} and c at fixed v_{α}), rather than the spread in proxy values at fixed M_* . That $\sigma(\mathcal{D})_1$ and σ_{tot}^2 are significantly overpredicted even without any scatter in the galaxy–halo connection demonstrates the extraordinary tightness of the MDAR. Since AM scatter = 0 is in any case ruled out by clustering (Lehmann et al. 2015), however, we will not consider this model further. As in Desmond & Wechsler (2016), we find also that the effect of varying α within the limits set by clustering measurements is small and does not significantly impact any of our statistics. We therefore conclude that varying the AM parameters cannot substantially improve the MDAR prediction.

We explore next the effect of modifications to the halo density profile due to disk formation, as parameterized by ν . The excessive value of $\langle \mathcal{D} \rangle_1$ in the fiducial model, in addition to $\langle \Delta(\mathcal{D})_r \rangle$ being too low, suggests that the degree of halo expansion corresponding to $\nu = -0.5$ is insufficient. We therefore show in Fig. 5(b) and row 4 of Tables 3–5 the results of changing ν to -1 , roughly the lowest value deemed plausible by Desmond & Wechsler 2015. This corresponds to more dark matter being expelled from the baryon-dominated inner regions of galaxies. Although $\langle \mathcal{D} \rangle_1$, $\langle \mathfrak{a} \rangle$, \mathcal{F}_+ and $\langle \Delta(\mathcal{D})_r \rangle$ all move closer to their observed values, they remain discrepant with the data. This suggests – at least within the parameter space spanned by our implementation – that

feedback is unlikely to resolve the low- a discrepancies. For reference, we show in the 5th row of Tables 3–5 the results of a model with standard adiabatic contraction ($\nu = 1$). In accordance with many studies in the literature, this clearly generates an excess of dynamical mass within the regions probed by kinematic measurements.

The scatter in the theoretical MDAR may be more efficiently reduced by imposing a correlation between galaxy morphology and halo concentration, effectively situating the late-type SPARC galaxies in haloes less concentrated than average. As described in Section 3.1, this may be achieved by removing at each stellar mass some fraction f of the highest concentration haloes before assigning haloes to the mock galaxies. The blue lines in Fig. 3 show the mean MDAR and its dispersion when the 80 per cent of highest concentration haloes at each stellar mass are removed from the theoretical parent population (i.e. $f = 0.8$; see also the 6th row of Tables 3–5). This is found to be the approximate value required for the predicted $\langle \mathcal{D} \rangle_1$ and $\sigma(\mathcal{D})_1$ to be consistent with that observed. By reducing mass discrepancies across the MDAR, this modification to the effective host halo population also reduces $\langle \mathfrak{a} \rangle$ and \mathcal{F}_+ . In addition, both $\langle \Delta(\mathcal{D})_{M_*} \rangle$ and $\langle \Delta(\mathcal{D})_{\Delta M_{\text{gas}}} \rangle$ are increased. This occurs because lower concentration galaxies have relatively more dark matter mass at large radius, while the rotation curves of galaxies with higher gas or stellar mass tend to be probed out to larger radii in the data. Hence the average \mathcal{D} of high M_* and M_{gas} galaxies are increased relative to those with low values. This effect corresponds also to a large increase in $\langle \Delta(\mathcal{D})_r \rangle$, bringing it into agreement with the observed value. We discuss this model further in Section 5.3.

As an alternative selection model, we report in row

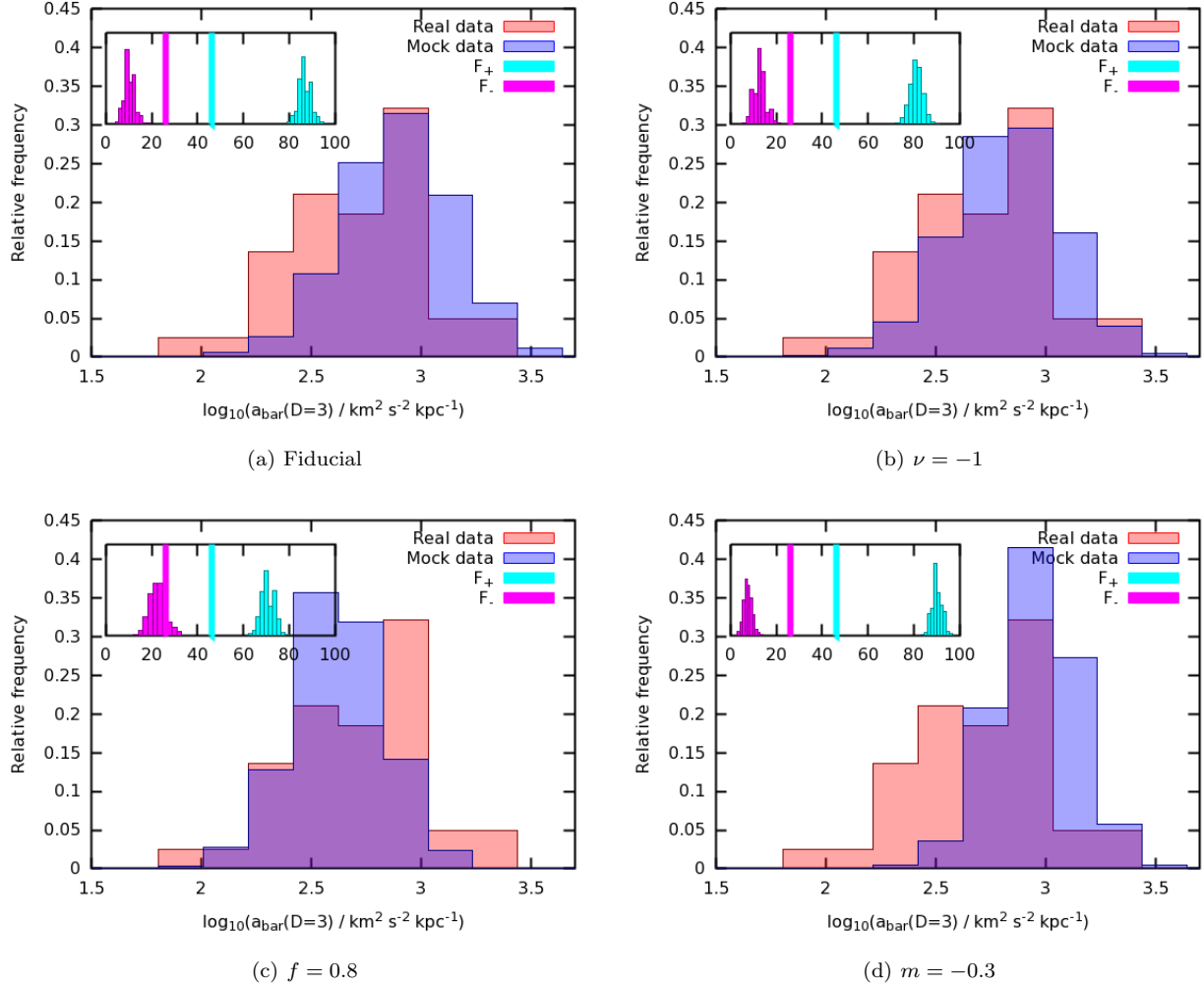


Figure 5. The predicted (blue) and observed (red) values of the acceleration (denoted a in the text) at which the mass discrepancy crosses $D = 3$. This is a proxy for the “characteristic acceleration” at which dark matter becomes unimportant. The blue histograms combine the results of all 2000 Monte Carlo realisations of the model. The inset shows the number of galaxies in each realisation with all measured points above $D = 3$ (cyan; \mathcal{F}_+), and below $D = 3$ (magenta; \mathcal{F}_-), compared to the values in the real data (vertical lines). These galaxies are excluded from the main histograms. The different panels correspond to models with individual deviations from the fiducial case, as labelled. The values of a in the real and mock data sets are similar, indicating that if the former are said to exhibit a “characteristic acceleration scale,” the latter should be too.

7 of Tables 3-5 the case in which each SPARC galaxy is required to occupy a distinct halo that is not located inside the virial radius of a larger halo. We find a moderate reduction in both $\langle D \rangle$ and $\sigma(D)$ across the acceleration range, showing that subhaloes have larger D on average. Changes to $\langle \Delta(D)_X \rangle$ are small, and there is a negligible difference in statistics pertaining to the characteristic acceleration scale. In terms of its effect on the MDAR, this is a middle ground between the fiducial model of Section 4.1 and the $f = 0.8$ model described above.

None of the model alterations examined so far have had a significant impact on $\langle \Delta(D)_{\Delta R_d} \rangle$ (Table 5, column 4), which has remained in all cases at least $2-3\sigma$ too high.

This indicates that larger galaxies at fixed stellar mass ought to reside in less massive haloes than have been assigned by the model, i.e. that R_d as well as M_* ought to correlate with halo c and M_{vir} . We anticipated this possibility with the size-concentration correlation model described in Section 3.1. We now consider the case $m < 0$, and tune m until the discrepancy in $\langle \Delta(D)_{\Delta R_d} \rangle$ is removed. We find $-0.5 \lesssim m \lesssim 0$ for the observed value of $\langle \Delta(D)_{\Delta R_d} \rangle$ to lie within the 95 per cent confidence interval of the theoretical prediction, and display the best-fitting case $m = -0.3$ in Figs. 3-7 and row 8 of Tables 3-5. This result suggests that in principle there is sufficient in-

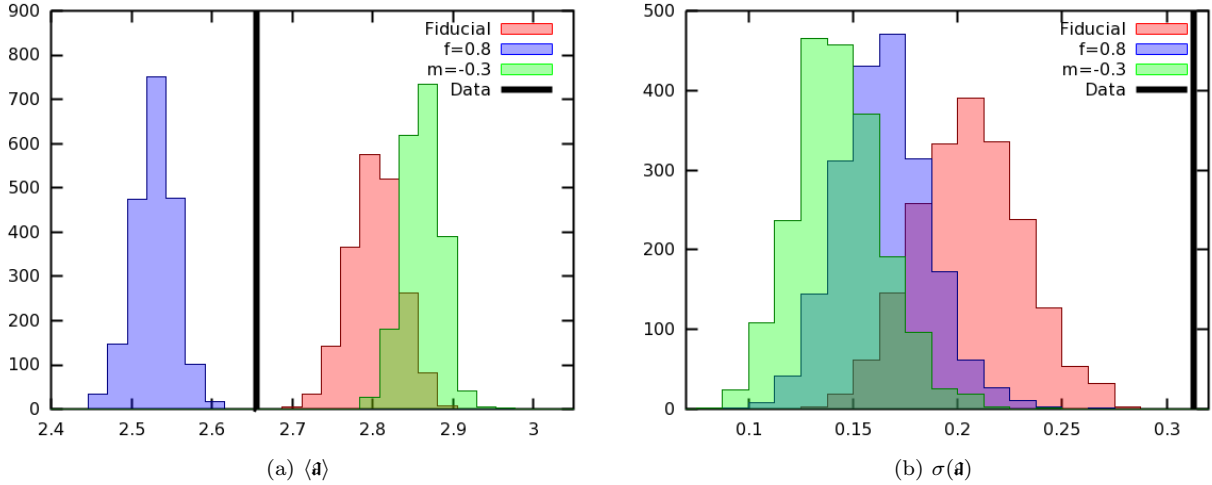


Figure 6. Histograms of the average (Fig. 6(a)) and standard deviations (Fig. 6(b)) of the “characteristic acceleration” a of galaxies within a mock data set, compared to that of the real data in black. While different model assumptions bracket the observed value of $\langle a \rangle$, the characteristic acceleration is in all cases *more* uniform in the mock than real data, as evidenced by a lower value of $\sigma(a)$.

formation in the MDAR to determine the correlation of galaxy size with halo properties at fixed stellar mass.

This correlation has two further consequences. First, since a galaxy of given size can no longer occupy a halo with any concentration, the spread in \mathcal{D} is lowered, leading to a reduction in both $\sigma(\mathcal{D})_1$ and σ_{tot}^2 . These remain in disagreement with the observed values, however, even when the correlation between c and ΔR_d is made very tight. This suggests that the spread in M_{vir} alone at fixed M_* , R_d and c overpredicts the MDAR scatter.

A second consequence of setting $m = -0.3$ is that $\langle \Delta(\mathcal{D})_{\Delta M_{\text{gas}}} \rangle$ is reduced (Fig. 7(c)). This is because R_d and M_{gas} are correlated at fixed M_* : larger galaxies have lower surface density and hence a lower star formation rate and greater ratio of M_{gas} to M_* . Reducing \mathcal{D} for larger galaxies therefore reduces it also for more gas-rich galaxies, so that $\langle \Delta(\mathcal{D})_{\Delta R_d} \rangle$ and $\langle \Delta(\mathcal{D})_{\Delta M_{\text{gas}}} \rangle$ shift together. In particular, when the predicted $\langle \Delta(\mathcal{D})_{\Delta R_d} \rangle$ agrees with the observations, $\langle \Delta(\mathcal{D})_{\Delta M_{\text{gas}}} \rangle$ is 1.3σ too low. Although this discrepancy is not statistically significant, taken at face value it suggests that more gas-rich galaxies ought to be assigned more massive haloes than gas-poor galaxies at fixed M_* and R_d . This could be achieved by abundance matching on total baryonic mass rather than stellar mass. Future analyses along these lines will determine whether this modification is necessary. We discuss the $\Delta R_d - \Delta c$ correlation further in Section 5.2.

5 DISCUSSION

5.1 Comparison with the literature

There have been few theoretical studies of the MDAR, and none to the level of detail presented here. Those

that do discuss the relation either use it to argue that Λ CDM-based models must not be able to account for the detailed dynamical properties of galaxies (Famaey & McGaugh 2012; Kroupa 2012; McGaugh 2015; Wu & Kroupa 2015), or, in reaction to such claims, that the relation does emerge from basic assumptions concerning galaxy formation (van den Bosch & Dalcanton 2000; Di Cintio & Lelli 2016). By means of detailed analysis of the statistical properties of the relation and its quantitative agreement with specific assumptions for the galaxy–halo connection, we intend our work to break this impasse and achieve a non-binary appreciation of the relation’s significance. In this section, we discuss the MDAR literature in light of our results. A recurring theme will be the assertion that a given model “can fit the MDAR” or “cannot in principle fit the MDAR,” where in fact the associated analysis warrants only the conclusion that it can or cannot fit one particular MDAR statistic – and even that not established quantitatively.

A series of papers (McGaugh & de Blok 1998; McGaugh 2004; Famaey & McGaugh 2012; McGaugh 2014, 2015) argue that the MDAR poses a serious fine-tuning problem for all Λ CDM-based galaxy formation models. In particular, it is claimed that neither the tightness of the observed MDAR nor the bottoming out of \mathcal{D} at high a can be accounted for. We confirm that the small scatter of the MDAR is a serious problem, although in our analysis the discrepancy is not as severe as suggested for example by fig. 3 of McGaugh (2015). This is because McGaugh (2015) considers as *a priori* plausible correlations between galaxy and halo variables that violate the assumptions of abundance matching; we on the other hand contend that the success of AM in matching to first order both clustering and kinematic statistics implies that the

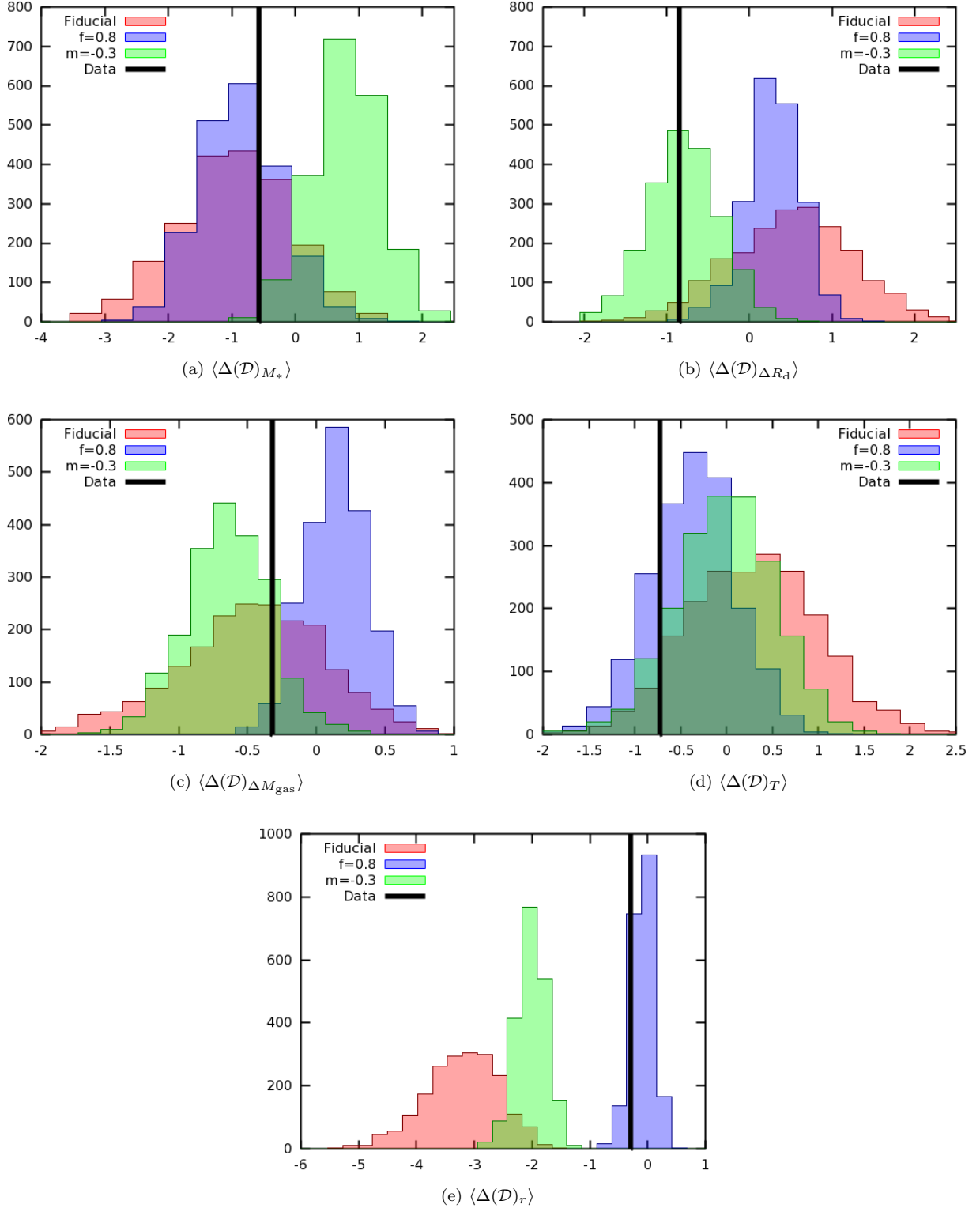


Figure 7. The weighted average difference in \mathcal{D} at fixed a ($\langle \Delta(\mathcal{D})_X \rangle$) between points with low and high values of various dynamically-relevant variables X : M_* (Fig. 7(a)), ΔR_d (Fig. 7(b)), ΔM_{gas} (Fig. 7(c)), Hubble type T (Fig. 7(d)), and galactocentric radius r (Fig. 7(e)). The histograms show the distributions for 2000 mock data sets drawn from the corresponding model, and the black line is the value in the real data. While $\langle \Delta(\mathcal{D})_{M_*} \rangle$, $\langle \Delta(\mathcal{D})_{\Delta M_{\text{gas}}} \rangle$ and $\langle \Delta(\mathcal{D})_T \rangle$ are matched well by a fiducial model, $\langle \Delta(\mathcal{D})_{\Delta R_d} \rangle$ provides evidence for a correlation between galaxy size and halo mass or concentration at fixed M_* , and $\langle \Delta(\mathcal{D})_r \rangle$ may imply strong concentration selection.

constraint it imposes on the galaxy–halo connection must obtain in any plausible galaxy formation scenario. That models inconsistent with the AM stellar mass–halo mass relation lie off the MDAR need not argue for a fine tuning problem with Λ CDM. They may instead be interpreted as a success of AM.

Further, we do not find low values of \mathcal{D} at high a to be problematic; indeed, given an amount of halo expansion compatible with the Tully–Fisher and Faber–Jackson relations, our models predict a *smaller* $\langle \mathcal{D} \rangle$ and $\sigma(\mathcal{D})$ at $a \gtrsim 2.8$ than is found in the data. We find in addition that the a values at which \mathcal{D} becomes small (in our case, $\mathcal{D} < 3$) are no less uniform in mock data than real data, and are clustered around a comparable central value. This success derives from the stellar-to-halo mass fractions of AM, combined with halo expansion and realistic galaxy sizes and baryonic mass profiles. If $\langle a \rangle$ and $\sigma(a)$ adequately capture the meaning of the terms “acceleration scale” or “characteristic acceleration,” we conclude that if present in the data these are present also in the mocks. That the acceleration scale of dark matter is around $c H_0$ is perhaps not so surprising if we consider that the average dark matter density is an $\mathcal{O}(1)$ multiple of ρ_{crit} , which is proportional to H_0^2 .

Nevertheless, many of the claims of Famaey & McGaugh (2012), McGaugh (2014) and McGaugh (2015) are borne out by our investigation. Not only are $\langle \mathcal{D} \rangle$, $\sigma(\mathcal{D})_1$ and σ_{tot}^2 naturally overpredicted, they remain so under highly conservative assumptions about galaxy formation, including no scatter in the galaxy–halo connection and a significant reduction in the spread of halo concentrations associated with a galaxy of fixed M_* and R_d . Furthermore, the details of the transition region from baryon to dark matter domination (as quantified by \mathcal{F}_+ and \mathcal{F}_-) are not understood, and \mathcal{D} is indeed compatible with being a function of a alone ($|\langle \Delta(\mathcal{D})_x \rangle| < 1$). Our analysis therefore serves to refine and focus questions concerning the compatibility of the MDAR with concordance cosmology.

van den Bosch & Dalcanton (2000) are concerned in part to show that galaxy formation scenarios with correct phenomenology in other respects must fit the MDAR. They present a model with feedback parameters tuned to match the Tully–Fisher relation, among others, and use it to generate 40 mock galaxies which they sample at regular intervals to produce a theoretical MDAR. They find that \mathcal{D} is a tighter function of a than r or V , and that it tends to 1 at high a . They claim on the basis of these results that the model successfully exhibits a “characteristic acceleration scale.” Although our study qualitatively agrees with several results of van den Bosch & Dalcanton (2000), we believe their claim of success to be too strong – such a conclusion could only be supported by a statistical analysis in which a mock data set with all the important features of the observed MDAR is not extraordinary given the parent galaxy–halo population. In particular, claiming success for *any* reasonable model

precludes using the relation to constrain models, which we believe we have shown to be both possible and fruitful.

Wu & Kroupa (2015) examine the MDAR of galaxies produced in several CDM and WDM hydrodynamical simulations, and conclude that the predicted and observed relations are incompatible. This conclusion is supported by an application of the Wilcoxon signed rank test, which quantifies the agreement of the ranks of \mathcal{D} in the observed and simulated data at given a . Although this test clearly demonstrates that the expected MDAR is on the whole normalised too high (a conclusion corroborated here), we caution that it need not be considered as decisive as the authors claim: since \mathcal{D} is reduced to its rank, a simulated MDAR consistently lying only slightly above the observations will appear as incompatible with them as one lying much higher, despite the fact that uncertainties in either data set may suffice to make them fully compatible according to any goodness-of-fit test that uses \mathcal{D} directly. Furthermore, the failure of individual simulations does not imply impossibility within the simulational framework. We suspect in addition that Wu & Kroupa (2015) use MOND mass-to-light ratios, which have no justification in Λ CDM. Nevertheless, we concur that the scatter in the expected MDAR is on the whole too high, and for the reasons given: there is a large spread in halo properties for given baryonic properties. We have placed this discrepancy on firm numerical footing, and furthermore brought to light the conditions required for a quantitative solution. Whether or not such conditions may be reasonably achieved by hydrodynamical simulations in Λ CDM remains to be seen.

Di Cintio & Lelli (2016) construct a semi-empirical model for the MDAR using average galaxy scaling relations from observations and halo scaling relations from N-body simulations. Although similar in spirit, our methodology improves upon that of Di Cintio & Lelli (2016) in several ways: we use an AM model that matches clustering measurements, we consider selection effects and correlations of halo variables with galaxy properties besides stellar mass, we give mock galaxies M_{gas} , R_d , $R_{d,\text{gas}}$ and $V_{\text{bar}}^2(r)$ values identical on a galaxy-by-galaxy basis with the data and sample their rotation curves at the same radii, we take the correlations between halo variables directly from a state-of-the-art N-body simulation rather than approximating them by power-laws with fixed log-normal scatter, and finally we make quantitative comparisons. While a confirmation of the qualitative results of van den Bosch & Dalcanton (2000) with updated measurements is valuable, Di Cintio & Lelli (2016) do not investigate the relation in sufficient detail to claim that all its pertinent aspects arise in Λ CDM.

Finally, Santos-Santos et al. (2016) compare the observed MDAR to that of 22 galaxies generated by the MaGICC and CLUES hydrodynamical simulations. Although the shape and scatter of the relation cannot be quantified with such a small sample, both seem to be in approximate agreement with the observations. With ref-

erence to analyses of this type, we argue that an empirical framework which offers complete transparency concerning its constituent elements provides a better handle on the aspects of the galaxy–halo connection responsible for important features of the predicted MDAR. Nevertheless, hydrodynamical simulations will produce correlations between galaxy and halo variables that lie outside our parameterizations, making a direct comparison with the MDAR valuable and complementary to our approach. We hope that future comparisons will utilise the statistics we have developed.

5.2 Parameter constraints and model requirements

The MDAR imposes several interesting constraints on AM-based galaxy formation models in Λ CDM, and provides evidence concerning a number of important correlations of the galaxy–halo connection. We discuss these issues here.

First, in agreement with Borriello et al. (2003), Dutton et al. (2007, 2013), Desmond & Wechsler (2015, 2016) and Di Cintio & Lelli (2016), the observed \mathcal{D} values fit more comfortably with expanded than contracted haloes: a high value of ν (such as that corresponding to standard adiabatic contraction) degrades the fit for the majority of our statistics. We find little sensitivity to the AM parameters within the ranges allowed by clustering measurements, although more generally the tightness of the MDAR argues for a small AM scatter. We find no evidence from $\langle \Delta(\mathcal{D})_{M_*} \rangle$ for deviations from the AM stellar mass–halo mass relation, and at best weak evidence from $\langle \Delta(\mathcal{D})_{\Delta M_{\text{gas}}} \rangle$ that AM based on total baryonic mass would perform better than the conventional stellar mass-based scheme. In addition, the agreement of $\langle \Delta(\mathcal{D})_T \rangle$ with our fiducial model suggests that galaxies of different Hubble type at fixed M_* do not reside in haloes with markedly different dynamical properties. We note however that the SPARC sample does not include any true early-type galaxies, and hence we cannot use this statistic to rule out the scenario in which the haloes of galaxies earlier than S0 differ substantially from those later.

The small offset between the MDARs of galaxies with the same stellar mass but different size requires at the 2σ level that lower surface brightness galaxies be placed in less massive or less concentrated haloes than is allowed for by standard AM. We have constructed a simple toy model for such a relation, and found that the observed value of $\langle \Delta(\mathcal{D})_{\Delta R_d} \rangle$ implies an average correlation $\Delta c \propto m \cdot \Delta R_d$, with $-0.5 \lesssim m \lesssim 0$ (95 per cent confidence) and best-fit value $m = -0.3$. The weakness of this correlation lends justification to the assumption used in many semi-analytic and empirical models that galaxy size is uncorrelated with halo properties at fixed M_* (e.g. Dutton et al. 2011, 2013; Desmond & Wechsler 2016; Di Cintio & Lelli 2016), and indeed models that make this assumption yield approximate agreement

with observed $\Delta V - \Delta R$ correlations (e.g. the tilt of the Fundamental Plane in the case of Dutton et al. 2013 and Desmond & Wechsler 2016) while those that impose strong $\Delta R_d - \Delta c$ or $\Delta R_d - \Delta M_{\text{vir}}$ correlations *a priori* do not (e.g. the correlation of velocity and size residuals in Desmond & Wechsler 2015). We stress however that the correlation between galaxy size and halo properties has important dynamical consequences and no strong prior (indeed, it is predicted by the celebrated Mo et al. 1998 model), and should therefore be explicitly considered in any galaxy formation model that seeks to explain galaxies' $M - V - R$ scaling relations. In an upcoming paper (Desmond et al. 2016, in prep), we will show that the EAGLE hydrodynamical simulation (Schaye et al. 2015) produces a $\Delta R_d - \Delta c$ correlation in approximate agreement with both MDAR and Tully–Fisher statistics, although the velocity and size residuals remain somewhat too strongly anticorrelated.

Remarkably, the “characteristic acceleration” at which \mathcal{D} becomes small is predicted to be no less uniform than that observed for all the models we consider, and hence the presence of this feature cannot be used to constrain the theory. We could not find any plausible choice for the galaxy–halo connection that significantly breaks this agreement (except perhaps the case of strong halo contraction).

Within the context of our framework, $\langle \mathcal{D} \rangle_1$, $\sigma(\mathcal{D})_1$, σ_{tot}^2 and $\langle \Delta(\mathcal{D})_r \rangle$ may argue for the SPARC galaxies occupying a subset of the total halo population highly biased in concentration or mass. We discuss the plausibility of such a model further in the following section.

5.3 Remaining problems

We have identified several aspects of the MDAR that cannot be matched – or can be matched only with extreme difficulty – in our framework. Foremost among these is the scatter, which we find to be too high in the theory both at low a ($\sigma(\mathcal{D})_1$) and in an averaged sense (σ_{tot}^2), regardless of the details of the AM scheme, the halo response to disk formation, and the correlation between galaxy size and halo concentration at fixed stellar mass. This is a particularly pressing problem because AM imposes a tight galaxy–halo connection by construction, and there is no guarantee that a full galaxy formation theory would naturally produce a correlation between M_* and v_α with only ~ 0.16 dex scatter. Indeed, the MDAR scatter is overpredicted even in the case of a perfectly monotonic galaxy–halo connection, when AM scatter is switched off. In addition, we have neglected observational uncertainties from disc inclination, mass-to-light ratio, distance, and three dimensional baryon structure, which would increase the intrinsic tightness of the relation still further. Finally, we have been careful to ensure that there are no differences between the local baryonic properties of mock and real galaxies or the radii at which their rotation curves are sampled, both of which could artificially

inflate the predicted scatter. Our conclusions concerning $\sigma(\mathcal{D})$ ought therefore to be highly conservative. The unexpected regularity of galaxy kinematics has been noted previously in the context of the baryonic Tully–Fisher relation, most recently for the SPARC sample in Lelli, McGaugh & Schombert (2016a).

A possible solution to this problem is to suppose that the SPARC galaxies occupy a substantially biased subset of the full halo population. We find that excluding the $f \approx 80$ per cent of haloes with highest concentration at each stellar mass reduces $\sigma(\mathcal{D})_1$ and σ_{tot}^2 to acceptable levels, in addition to mitigating the offset of the \mathcal{D} values of low and high r points, as measured by $\langle \Delta(\mathcal{D})_r \rangle$. In line with Desmond & Wechsler (2015), it is tempting to interpret this as a correlation between morphology and host halo structure. That such a model may be fleshed out in detail, however, is doubtful, for four reasons:

(i) The SPARC galaxies span the range from S0 to Im/BCD, a morphological subset that accounts for $\gg 20$ per cent of the total galaxy population (e.g. Bamford et al. 2009; Henriques et al. 2015).

(ii) Even supposing one could justify discarding 80 per cent of haloes, it is implausible that these should be the exact haloes with highest concentration. A non-monotonic selection function would require a further increase in f to be effective.

(iii) When the fraction of haloes removed is constant over stellar mass, \mathcal{D} is also reduced for $a > 2.8$ where it already lies below the observed values in the fiducial model. Since the high-acceleration regime is mostly populated by high-mass galaxies, this would suggest that the fraction of haloes removed ought to be lower at higher M_* , yet the fraction of early-types rises with M_* .

(iv) As discussed in Section 4, the agreement between the observed and predicted $\langle \Delta(\mathcal{D})_T \rangle$ reveals that the average difference in the masses or mass distributions of haloes of galaxies with different morphology within the SPARC sample cannot be large. Forcing galaxies of earlier type to inhabit more concentrated haloes would reduce $\langle \Delta(\mathcal{D})_T \rangle$, probably out of consistency with the data.

The second most significant challenge is the excess $\langle \mathcal{D} \rangle$ predicted at low a . This continues a long line of results indicating that the amount of dark matter in galaxies predicted by galaxy formation models applied to N-body simulations is on the whole too high, a problem which manifests itself in many and varied forms (e.g. Klypin et al. 1999; Moore et al. 1999; Bournaud et al. 2007; Kuzio de Naray & Spekkens 2011; Boylan-Kolchin et al. 2011, 2012; Karachentsev 2012; Weinberg et al. 2013). We note that while this discrepancy can be remedied in the case of galaxy 1-point scaling relations – the Tully–Fisher and Faber–Jackson relations – by means of a global halo expansion parameterized in the same way as adiabatic contraction (Desmond & Wechsler 2015, 2016), the radius-dependent information in the MDAR reveals that this method is inadequate in detail.

No value of ν in the range that correctly predicts the Tully–Fisher normalisation, for example, can generate a value of $\langle \mathcal{D} \rangle_1$ as low as that observed.

Low acceleration points come from low surface brightness galaxies (LSBs) and the outer regions of high surface brightness galaxies (HSBs). Two unique features of the SPARC sample are its high proportion of LSBs and its wide range of stellar mass (down to $M_* = 10^{6.7} M_\odot$). Tully–Fisher and Faber–Jackson data sets, on the other hand, tend to be dominated by HSBs and extend no lower than $M_* \approx 10^9 M_\odot$. The excess mass discrepancy at low a is largely due to low mass LSBs: these galaxies are placed in haloes that are too massive. There are hints that this would impact the baryonic Tully–Fisher relation were it extended to low mass (Desmond 2012; Papastergis et al. 2016), and the discrepancy receives full expression in the Too Big To Fail (Boylan-Kolchin et al. 2011, 2012) and cusp-core (de Blok 2010) problems at the dwarf scale. Potential solutions to those problems apply here also, most prominently the possibility of strong feedback. Indeed, the low value of $\langle \Delta(\mathcal{D})_r \rangle$ in the fiducial model (indicating an excess of dark matter at low over high radii) may also be evidence of feedback: a successful scheme would not only need to move dark matter outwards, but do so preferentially in low mass, low surface brightness galaxies. If feedback is powered by star formation, it might be thought that such galaxies ought to have a *smaller* impact on their haloes, although some simulations (e.g. Di Cintio et al. 2014) do predict such an effect. We stress however that simply reducing \mathcal{D} by moving dark matter outwards is not enough: the spread in \mathcal{D} must also be reduced, for example by homogenising the haloes. It is unclear whether this is expected.

The discrepancy in $\langle \mathcal{D} \rangle_1$ may also be alleviated by modifying the galaxies’ stellar masses. We have assumed that the stellar masses assigned by AM are identical to those of the SPARC sample, although in practice they have been derived using different assumptions for galaxy photometry, mass-to-light ratios and IMF. Since the AM stellar-to-halo mass ratio peaks around $M_* = 10^{10.5} M_\odot$, if the galaxies at the low-mass end of the SPARC sample in fact correspond to galaxies of higher stellar mass in our model then the predicted mass discrepancies would be reduced at low a . This effect is degenerate with a modification to AM which places lower mass galaxies in less massive haloes. It is also possible that extrapolating the stellar and halo mass function below their resolution limits ($M_* \approx 10^9 M_\odot$) could introduce systematic errors at the low- a end of the MDAR.

If none of these modifications prove effective, non-standard dark matter interactions may be required (e.g. Blanchet & Le Tiec 2008; Rocha et al. 2013; Suárez, Robles & Matos 2014; Khouri 2016).

Four more MDAR statistics cannot be matched at the 95 per cent level within our framework: the high-acceleration average mass discrepancy and scatter ($\langle \mathcal{D} \rangle_{16}$ and $\sigma(\mathcal{D})_{16}$) and the number of galaxies within a given

data set with points on either side of $\mathcal{D} = 3$ (\mathcal{F}_+ and \mathcal{F}_-). We doubt however that these discrepancies provide additional information on the galaxy–halo connection: $\langle \mathcal{D} \rangle_{16}$ and $\sigma(\mathcal{D})_{16}$ likely point to additional measurement uncertainty, and correct prediction of \mathcal{F}_+ and \mathcal{F}_- may well follow from success in matching $\langle \mathcal{D} \rangle$ at low a .

5.4 Implications for MOND

Since the MOND prediction for the MDAR has less freedom than that of Λ CDM, the relation offers less potential to constrain it; on the flip-side, this makes the MOND prediction easier to rule out. We note three ways in which our analysis has relevance for MOND.

- *Prima facie*, $\langle \mathcal{D} \rangle > 1$ at $a > a_0$ implies the existence of missing mass in the Newtonian regime, violating a basic principle of MOND. Since we have shown that this is equally unexpected for AM, however, it is likely due to additional measurement error. This may derive from uncertainties in disc inclination, mass-to-light ratio, distance, or the three dimensional distributions of the baryons.

- Absent systematic uncertainty, \mathcal{D} depends *only* on a in MOND, and hence MDAR residuals may not correlate with any other variable. In our analysis, this implies $\langle \Delta(\mathcal{D})_X \rangle = 0$ for each of $X = \{M_*, \Delta R_d, \Delta M_{\text{gas}}, T, r\}$. As noted in Section 4.1, the magnitudes of each of these variables in the data are < 1 and hence compatible with 0 within the measurement uncertainty, supporting the hypothesis that \mathcal{D} is a function of a alone. This finding is made somewhat more significant by the fact that our model predictions for $|\langle \Delta(\mathcal{D})_X \rangle|$ significantly exceed 1 in some cases.

- In a Bayesian model comparison sense, an increase in the evidence achievable by Λ CDM models disfavours MOND, and vice versa. We have shown that the presence of a “characteristic acceleration” in the MDAR cannot discriminate against AM mocks. On the other hand, we have considerably strengthened the argument that the scatter in the relation is lower than predicted by standard galaxy formation, especially at low a .

6 CONCLUSION

The MDAR provides a map between the distribution of a galaxy’s baryonic and dark matter, and therefore contains crucial information about the galaxy–halo connection. In this paper we have laid the groundwork for extracting this information for use in evaluating models of galaxy formation. We have analysed the MDAR using a set of 14 statistics that quantify its four most important features: its shape, its scatter, the presence of a “characteristic acceleration” beyond which mass discrepancy consistently goes to ~ 1 , and the correlation of its residuals with other galaxy properties. In addition to using

these statistics to focus discussion of the observed relation itself, we have engaged them to construct a data-driven framework for the galaxy–halo connection. Building upwards from the simplest case of stellar mass-based abundance matching in Λ CDM, we have successively incorporated selection effects, a correlation between galaxy size and halo concentration, and a mass-dependent prescription for the impact of disk formation on halo density profiles. Comparing to data from the SPARC sample, our most significant findings are the following.

- A basic AM model readily accounts for several features of the MDAR, including its approximate overall shape, its small scatter at high acceleration, and the independence of its residuals on stellar mass. In addition, we find no grounds for the claim that the acceleration at which the mass discrepancy becomes low is more uniform in the data than is expected in theory (a “characteristic acceleration scale”).

- Nevertheless, the predicted MDAR has significantly too high a normalisation and scatter at low a . This remains true under highly conservative assumptions for galaxy formation, including no scatter in the galaxy–halo connection and a significant reduction in the spread of halo concentrations associated with a galaxy of fixed M_* and R_d . This indicates too much dark matter predicted in the outer regions of high surface brightness galaxies and (especially) in low surface brightness galaxies, and too large a variation among halo properties. In addition, dark matter is more concentrated towards the centres of galaxies than the MDAR suggests. These discrepancies argue for halo expansion in response to disk formation, and a quantitative resolution requires also the exclusion of a large fraction (~ 80 per cent) of the haloes with highest concentration at each stellar mass.

- The MDAR may be used to detect correlations of halo properties with (at least) three galaxy properties at fixed stellar mass: gas mass, disc size, and Hubble type. Our analysis suggests at the $\sim 2\sigma$ level that galaxy size is anticorrelated with halo concentration at fixed stellar mass. There exists in addition weak evidence in favour of basing AM on total baryonic mass rather than stellar mass, but negligible direct evidence that the haloes of early-type galaxies have systematically different properties than those of later type.

We hope that this work will stimulate interest in the MDAR as a source of information about the galaxy–halo connection. Looking forward, we identify three ways in which further progress could be made. First, additional models and assumptions need to be tested against the relation to the level of rigour achieved here. It is unclear to what extent the outputs of many hydrodynamical simulations or semi-analytic models, for example, are consistent with MDAR statistics. Specific implementations of the correlations of halo properties with galaxy variables besides M_* (e.g. AM using total baryonic mass, or the angular momentum partition model of Mo et al. 1998) should

be tested individually. Second, a firmer theoretical basis needs to be given for the empirical galaxy–halo correlations argued for by the MDAR; this may be possible by mapping hydrodynamical simulations onto phenomenological frameworks such as ours. Finally, an increase in the size and precision of MDAR data sets may be expected to yield a considerable gain in the constraining power of analyses of this type, pinning down the values of the statistics in the real data and reducing the widths of their distributions in the mock data. The full power of the MDAR likely remains to be harnessed.

ACKNOWLEDGMENTS

I thank Xavier Hernandez, Federico Lelli, Stacy McGaugh and Risa Wechsler for fruitful discussions during the course of this work, and Simon Foreman for comments on the manuscript. I am particularly grateful to Federico Lelli for access to and guidance with the SPARC data.

This work made use of one of the Dark Sky simulations, which were produced using an INCITE 2014 allocation on the Oak Ridge Leadership Computing Facility at Oak Ridge National Laboratory. I thank the Dark Sky collaboration for creating and providing access to this simulation, and Sam Skillman and Yao-Yuan Mao for running ROCKSTAR and CONSISTENT TREES on it, respectively. Additional computation was performed at SLAC National Accelerator Laboratory.

This work received partial support from the U.S. Department of Energy under contract number DE-AC02-76SF00515.

REFERENCES

Bamford S. P. et al., 2009, MNRAS, 393, 1324
 Behroozi P. S., Conroy C., Wechsler R. H., 2010, ApJ, 717, 379
 Behroozi P. S., Wechsler R. H., Wu H.-Y., 2013, ApJ, 762, 109
 Behroozi P. S., Wechsler R. H., Wu H.-Y., Busha M., Klypin A., Primack J., 2013, ApJ, 763, 18
 Behroozi P. S. et al., 2015, MNRAS, 450, 1546
 Bernardi M., Meert A., Sheth R. K., Vikram V., Huertas-Company M., Mei F., Shankar F., 2013, MNRAS, 436, 697
 Blanchet L., Le Tiec A., 2008, Phys. Rev. D, 78, 024031
 Blumenthal G. R., Faber S. M., Flores R., Primack J. R., 1986, ApJ, 301, 27
 Borriello A., Salucci P., Danese L., 2003, MNRAS, 341, 1109
 Bournaud F., 2007, Science, 316, 1166
 Boylan-Kolchin M., Bullock J. S., Kaplinghat M., 2011, MNRAS, 415, L40
 Boylan-Kolchin M., Bullock J. S., Kaplinghat M., 2012, MNRAS, 422, 1203
 Conroy C., Wechsler R. H., Kravtsov A. V., 2006, ApJ, 647, 201
 Conroy C., van Dokkum P. G., 2012, ApJ, 760, 71
 de Blok W. J. G., 2010, Adv. Astron., 2010, 789293
 Desmond H., 2012, preprint (arXiv:1204.1497)
 Desmond H., Wechsler R. H., 2015, MNRAS, 454, 322
 Desmond H., Wechsler R. H., 2016, preprint (arXiv:1604.04670)
 Di Cintio A., Brook C. B., Dutton A. A., Macciò A. V., Stinson G. S., Knebe A., 2014, MNRAS, 441, 2986
 Di Cintio A., Lelli F., 2016, MNRAS, 456, L127
 Dutton A. A., van den Bosch F. C., Dekel A., Courteau S., 2007, ApJ, 654, 27
 Dutton A. A. et al., 2011, MNRAS, 416, 322
 Dutton A. A., Macciò A. V., Mendel J. T., Simard L., 2013, MNRAS, 432, 2496
 Famaey B., McGaugh S. S., 2012, Living Rev. Relativ., 15, 10
 Gnedin O. Y., Kravtsov A. V., Klypin A. A., Nagai D., 2004, ApJ, 616, 16
 Gnedin O. Y., Ceverino D., Gnedin N. Y., Klypin A. A., Kravtsov A. V., Levine R., Nagai D., Yepes G., 2011, preprint, (astro-ph/1108.5736)
 Governato F. et al., 2010, Nature, 463, 203
 Guo Q., White S., Li C., Boylan-Kolchin M., 2010, MNRAS, 404, 1111
 Hearn A. P., Watson D. F., 2013, MNRAS, 435, 1313
 Hearn A. P., Watson D. F., Becker M. R., Reyes R., Berlind A. A., Zentner A. A., 2014, MNRAS, 444, 729
 Henriques B. M. B., White S. D. M., Thomas P. A., Angulo R., Guo Q., Lemson G., Springel V., Overzier R., 2015, MNRAS, 451, 2663
 Janz J., Cappellari M., Romanowsky A. J., Ciotti L., Alabi A., Forbes D., 2016, preprint (arXiv:1606.05003)
 Jennings E., Wechsler R. H., Skillman S. W., Warren M. S., 2016, MNRAS, 457, 1076
 Karachentsev I. D., 2012, Astrophysical Bulletin, 67, 123
 Khoury J., 2016, preprint (arXiv:1605.08443)
 Klypin A., Kravtsov A. V., Valenzuela O., Prada F., 1999, ApJ, 522, 82
 Kravtsov A. V., Berlind A. A., Wechsler R. H., Klypin A. A., Gottlober S., Allgood B., Primack J. R., 2004, ApJ, 609, 35
 Kroupa P., 2012, PASA, 29, 395
 Kuzio de Naray R., Spekkens K., 2011, ApJL, 741, L29
 Lehmann B. V., Mao Y.-Y., Becker M. R., Skillman S. W., Wechsler R. H., 2015, preprint (arXiv:1510.05651)
 Lelli F., McGaugh S. S., Schombert J. M., 2016, ApJL, 816, L14
 Lelli F., McGaugh S. S., Schombert J. M., 2016, preprint (arXiv:1606.09251)
 Mandelbaum R., Wang W., Zu Y., White S., Henriques B., More S., 2016, MNRAS, 457, 3200
 Mashchenko S., Wadsley J., Couchman H. M. P., 2008, Science, 319, 174
 McGaugh S. S., de Blok, W. J. G., 1998, ApJ, 499, 41

McGaugh S. S., 1999, Galaxy Dynamics - A Rutgers Symposium, 182, 528

McGaugh S. S., 2004, ApJ, 609, 652

McGaugh S. S., 2014, Galaxies, 2, 601

McGaugh S. S., 2015, Canadian Journal of Physics, 93, 250

Milgrom M., 1983, ApJ, 270, 365

Milgrom M., 1983, ApJ, 270, 371

Milgrom M., 1983, ApJ, 270, 384

Mo H.J., Mao S., White S.D.M., 1998, MNRAS, 295, 319

Moore B., Quinn T., Governato F., Stadel J., Lake G., 1999, MNRAS, 310, 1147

Moster B. P., Somerville R. S., Maulbetsch C., van den Bosch F. C., Macciò A. V., Naab T., Oser L., 2010, ApJ, 710, 903

Papastergis E., Adams E. A. K., van der Hulst J. M., 2016, preprint (arXiv:1602.09087)

Pontzen A., Governato F., 2012, MNRAS, 421, 3464

Reddick R. M., Wechsler R. H., Tinker J. L., Behroozi P. S., 2013, ApJ, 771, 30

Rocha M., Peter A. H. G., Bullock J. S., Kaplinghat M., Garrison-Kimmel S., Onorbe J., Moustakas L., 2013, MNRAS, 430, 81

Rodríguez-Puebla A., Avila-Reese V., Firmani C., Colín P., 2011, Rev. Mex. Astron. Astrofis., 47, 235

Sanders R. H., 1990, A&AR, 2, 1

Santos-Santos I. M., Brook C. B., Stinson G., Di Cintio A., Wadsley J., Domínguez-Tenreiro R., Gottlöber S., 2016, MNRAS, 455, 476

Schaye J. et al., 2015, MNRAS, 446, 521

Skillman S. W., Warren M. S., Turk M. J., Wechsler R. H., Holz D. E., Sutter P. M., 2014, preprint (arXiv:1407.2600)

Suárez A., Robles V. H., Matos T., 2014, Astrophysics and Space Science Proceedings, 38, 107

Tiret O., Combes F., 2009, A&A, 496, 659

Trujillo-Gómez S., Klypin A., Primack J., Romanowsky A. J., 2011, ApJ, 742, 16

van den Bosch F. C., Dalcanton J. J., 2000, ApJ, 534, 146

Warren M. S., 2013, Proceedings of the International Conference on High Performance Computing, Networking, Storage and Analysis, 72

Weinberg D. H., Bullock J. S., Governato F., Kuzio de Naray R., Peter A. H. G., 2013, preprint (arXiv:1306.0913)

Wojtak R., Mamon G. A., 2013, MNRAS, 428, 2407

Wu X., Kroupa P., 2015, MNRAS, 446, 330